ON TWO MOMENT SYSTEMS FOR COMPUTING MULTIPHASE SEMICLASSICAL LIMITS OF THE SCHRÖDINGER EQUATION

LAURENT GOSSE, SHI JIN, AND XIANTAO LI

ABSTRACT. Two systems of hyperbolic equations, arising in the multiphase semiclassical limit of the linear Schrödinger equations, are investigated. One stems from a Wigner measure analysis and uses a closure by the Delta functions, whereas the other relies on the classical WKB expansion and uses the Heaviside functions for closure. The two resulting moment systems are weakly and non-strictly hyperbolic respectively. They provide two different Eulerian methods able to reproduce superimposed signals with a finite number of phases. Analytical properties of these moment systems are investigated and compared. Efficient numerical discretizations and test-cases with increasing difficulty are presented.

1. INTRODUCTION

We aim at computing efficiently the semiclassical limits of the linear Schrödinger equation with high frequency WKB initial data,

$$i\epsilon\partial_t\psi^\epsilon + \tfrac{\epsilon^2}{2}\Delta\psi^\epsilon = V(\mathbf{x})\psi^\epsilon, \qquad \mathbf{x}\in\mathbb{R}^n, \tag{1}$$

$$\psi^\epsilon(\mathbf{x},0) = A_0(\mathbf{x})\mathrm{e}^{i\frac{S_0(\mathbf{x})}{\epsilon}}. \tag{2}$$

In (1) ψ^ϵ is the complex wave function, ϵ is the scaled Planck constant, and $V(\mathbf{x})$ stands for a smooth potential. In the semiclassical regime which corresponds to a small value of ϵ, the wave function $\psi^\epsilon(\mathbf{x},t)$ and its related physical observables exhibit oscillatory behavior with wave length $O(\epsilon)$. This may prevent any strong convergence as ϵ vanishes, as is well-known, [21, 31, 32].

To obtain physically correct observables numerically when $\epsilon\to 0$, a direct numerical discretization of (1)–(2) with a Cartesian grid requires the mesh size and time step to be $o(\epsilon)$ when a finite difference method is used [42]. The use of time-splitting spectral methods [3] can improve the mesh size to $O(\epsilon)$ and time step to $O(1)$. But still, these constraints make computations in the semiclassical regime prohibitively expensive, especially in several space dimensions.

A more subtle strategy seeks asymptotic solution in the limit $\epsilon\to 0$ by assuming the form of the solution to be $\psi^\epsilon(x,t) = A(x,t)\exp(iS(x,t)/\epsilon)$ (this is also called the Madelung transformation [41]). This is the classical WKB expansion which gives, to the leading order, an eikonal equation for the phase function S and a linear transport equation for the intensity (the square of the amplitude $|A|^2$, also called the position density), see [35] and §2.1:

$$\partial_t S + \frac{1}{2}|\nabla S|^2 + V(\mathbf{x}) = 0, \qquad \partial_t(|A|^2) + \nabla\cdot(|A|^2\nabla S) = 0. \tag{3}$$

* Research was supported in part by NSF grant DMS-0196106.

The eikonal equation is a nonlinear Hamilton-Jacobi equation. Even for smooth initial data, its solution may become singular in finite time, which corresponds to the focusing of the characteristic curves, *i.e.* the formation of a caustic. In fact, caustics do appear as soon as $\partial_{xx} S_0 < 0$ in some interval. Beyond this singularity, most of modern 'shock-capturing' numerical methods will select the very stable *viscosity solution* [15, 16], which differs significantly from the dispersive semiclassical limit, [21], since the viscosity solution violates the superposition principle, an essential property of the linear Schrödinger equation. In fact, beyond the caustics, solution becomes multivalued or multiphased, see [52, 34, 48]. Such multiphase solutions will be the subject of study in this paper, and the goal is to investigate and compare two Eulerian approaches to numerically compute these multiphase solutions.

We mention that $|A|^2$ can still be understood in the duality sense [7], and this direction has been investigated after [19, 50]. Precise results about (3) have been obtained in *e.g.* [29, 28].

In order to comply with the linear superposition principle for (1), one may track the characteristic curves of (3) and then deduce the geometric solution of the eikonal equation in (3). This Lagrangian method amounts to solving a set of ordinary differential equations along the characteristic curves, and is usually referred to as the *ray tracing* method. See [4, 5, 6] for the latest developments in this direction.

A mathematically convenient tool for studying the semiclassical limits is the Wigner transform [38, 22, 53], which is defined as

$$W[\phi,\psi](\mathbf{x},\mathbf{v},t) = \frac{1}{(2\pi)^n}\int_{\mathrm{R}^n} \mathrm{e}^{i\mathbf{v}\cdot\mathbf{y}}\phi\Big(\mathbf{x}-\frac{\epsilon\mathbf{y}}{2}\Big)\overline{\psi}\Big(\mathbf{x}+\frac{\epsilon\mathbf{y}}{2}\Big)d\mathbf{y}.$$

For ψ^ϵ satisfying (1), $W^\epsilon = W[\psi^\epsilon,\psi^\epsilon]$ can be shown to converge weakly towards a measure solution of the Liouville equation from classical mechanics:

$$\partial_t w + \mathbf{v}\cdot\nabla_{\mathbf{x}} w - \nabla V\cdot\nabla_{\mathbf{v}} w = 0. \tag{4}$$

As a linear kinetic equation, the Liouville equation naturally unfolds the caustics and therefore can generate the correct multiphase solutions *globally in time.*

Nevertheless, numerical computation of kinetic equations is still expensive and an appropriate *Maxwellian distribution* that can be used to close moment equations of the kinetic equation is desirable. This program, briefly outlined in §2.3–4, can be done in two ways. The first one is to use the fact that W^ϵ converges weakly, before the formation of caustics, to a so-called 'monokinetic density' [11, 13]–which is a delta measure, and then to study how to extend it to a 'multiphase density' beyond the caustic time. This strategy has been followed for instance in [17, 34], to derive the resulting (weakly) hyperbolic system satisfied by the corresponding moments. This approach will be referred to as the *delta closure* and the corresponding moment system will be called the δ-system.

Another one, proposed by Brenier and Corrias [12], takes for granted (3) and then uses Heaviside functions to close the kinetic equation (4). This provides a way to reconstruct the geometrical (multivalued) solution of the Burgers' equation beyond the shock. The resulting moment system is a (nonstrictly) hyperbolic system of balance laws in the ambient space. This approach will be referred to as the *Heaviside closure* and the resulting system will be referred to as the H-system.

Although the moment systems are seemingly quite different, they share some common properties. This will be studied in §3. In one space dimension, when the number of moments used within the closure process is sufficiently large, the

two systems are equivalent, as will be proved in §3.2. This statement is confirmed by the numerical computations of §5, using the numerical schemes constructed in §4. However, if the semiclassical limit of (1)–(2) develops more phases than the moments system can support, both closures amount to impose some singular source terms on the right-hand-side of the kinetic equation (4) and they have not been proved to generate the same analytical solutions. The numerical discretizations of these two schemes, using the schemes constructed in §4, give drastically different results, see Figs. 11, 12 (and also the results given in [47]).

The Wigner approach is naturally multidimensional: a two-dimensional moment system was given in [34]. It has not been numerically tested yet. The Brenier-Corrias' approach has not been extended to several space dimensions – it is theoretically possible but technically rather tedious since it needs a delicate ordering on the values of the velocities.

Since the δ-system is weakly hyperbolic, standard shock capturing schemes such as the Lax-Friedrichs scheme and the Godunov scheme face some numerical difficulties [9]. In addition, the fluxes maybe discontinuous across the caustics, and these discontinuities are *undercompressive shocks* as shown in §3, the numerical approximation of these moment systems is a delicate task. We use a kinetic scheme derived from the Liouville equation as in [34] for the δ-system. When the potential is nonconstant, we use a *well-balanced* idea introduced in [45] to incorporate the forcing term . For the H-system, a local Lax-Friedrichs scheme is used, which will also be coupled with the forcing term in a well-balanced way [24, 26]. We also give a new simple way to approximate the intensity, which results in a much better numerical resolution. These numerical schemes produce better numerical results those previously used for similar moment systems.

2. Two moment systems for multiphase solutions

2.1. **The Wigner measure and the delta-closure.** For smooth functions ϕ and ψ, rapidly decaying at infinity (more precisely, belonging to L. Schwartz's class $\mathcal{S}(\mathbb{R}^n)$), the Wigner distribution is defined as [53]:

$$W[\phi,\psi](\mathbf{x},\mathbf{v},t) = \frac{1}{(2\pi)^n}\int_{\mathbb{R}^n} \mathrm{e}^{i\mathbf{v}\cdot\mathbf{y}}\phi\left(\mathbf{x}-\frac{\epsilon\mathbf{y}}{2}\right)\overline{\psi}\left(\mathbf{x}+\frac{\epsilon\mathbf{y}}{2}\right)d\mathbf{y}. \tag{5}$$

When ψ^ϵ solves the Schrödinger equation (1), the Wigner distribution

$$W^\epsilon(\mathbf{x},\mathbf{v},t) = W[\psi^\epsilon,\psi^\epsilon]$$

solves the Wigner equation,

$$\partial_t W^\epsilon + \mathbf{v}\cdot\nabla_{\mathbf{x}} W^\epsilon - \Xi^\epsilon[V]W^\epsilon = 0, \tag{6}$$

where the linear operator Ξ can be written as

$$\Xi^\epsilon[V]W^\epsilon = \frac{i}{(2\pi)^n\epsilon}\int_{\mathbb{R}^n} \mathrm{e}^{i\mathbf{v}\cdot\mathbf{y}}\psi^\epsilon\left(\mathbf{x}-\frac{\epsilon\mathbf{y}}{2},t\right)\overline{\psi^\epsilon}\left(\mathbf{x}+\frac{\epsilon\mathbf{y}}{2},t\right)\left[V\left(\mathbf{x}+\frac{\epsilon\mathbf{y}}{2}\right)-V\left(\mathbf{x}-\frac{\epsilon\mathbf{y}}{2}\right)\right]d\mathbf{y}.$$

It can been shown (see for example [22]) that as $\epsilon\to 0$,

$$\Xi^\epsilon[V]W^\epsilon \to \nabla_{\mathbf{x}}V\cdot\nabla_{\mathbf{v}}w\,.$$

Altogether, in the limit $\epsilon\to 0$, the series of Wigner functions W^ϵ is weakly compact and converges towards the solution w of the classical Liouville equation,

$$\partial_t w + \mathbf{v}\cdot\nabla_{\mathbf{x}} w - \nabla_{\mathbf{x}}V\cdot\nabla_{\mathbf{v}} w = 0. \tag{7}$$

In addition, the Wigner transform of the initial wave function (2)

$$W^\epsilon(\mathbf{x},\mathbf{v},0)=\frac{1}{(2\pi)^n}\int_{\mathbb{R}^n}A_0(\mathbf{x}-\frac{\epsilon y}{2})\overline{A_0}(\mathbf{x}+\frac{\epsilon y}{2})\mathrm{e}^{i\mathbf{v}\cdot\mathbf{y}}\ \mathrm{e}^{-i\frac{S_0(\mathbf{x}+\frac{\epsilon\mathbf{y}}{2})-S_0(\mathbf{x}-\frac{\epsilon\mathbf{y}}{2})}{\epsilon}}d\mathbf{y}$$

converges weakly to a classical particle of mass-velocity $(\rho_0,\mathbf{u}_0)$:

$$w(\mathbf{x},\mathbf{v},0)=\rho_0(\mathbf{x})\delta(\mathbf{v}-\mathbf{u}_0(\mathbf{x})), \tag{8}$$

where $\mathbf{u}_0=\nabla S_0$, $\rho_0=|A_0|^2$ and $\delta(\cdot)$ stands for the Dirac measure. This bridges the quantum mechanics and classical mechanics, as explained in [35]. Moreover, it was shown in [21] that the first two moments of W^ϵ converge also weakly towards those of w, ensuring the consistency of physical observables in the limit $\epsilon\to 0$. Before breakdown time t_b (when the first caustics forms), the solution keeps on being a so-called *monokinetic density*,

$$w(\mathbf{x},\mathbf{v},t)=\rho(\mathbf{x},t)\delta(\mathbf{v}-\mathbf{u}(\mathbf{x},t)). \tag{9}$$

Applying (9) to the Liouville equation (7) and taking the first two moments yield a closed system for ρ and $\mathbf{u}$

$$\begin{array}{rcl}\partial_t\rho+\nabla\cdot(\rho\mathbf{u}) & = & 0,\\ \partial_t(\rho\mathbf{u})+\nabla\cdot(\rho\mathbf{u}\otimes\mathbf{u})+\rho\nabla V & = & 0.\end{array} \tag{10}$$

These are the pressureless gas equations, which form a weakly hyperbolic system with only one characteristic speed $\mathbf{u}$, and its Jacobian matrix is similar to a Jordan block. Beyond the break time t_b the above ansatz (9) is no longer valid. Direct simulations of the pressureless gas system (10) using shock capturing techniques yield the viscosity solution[1], such as the δ-shock solution [9], which violates the superposition principle and does not provide the correct semiclassical limits of the linear Schrödinger equation.

In fact, the semiclassical solution displays multiphase phenomena once the single phase ansatz breaks down. If the total number of phases N is finite, the corresponding form of the density distribution, as proved in [34, 48], takes the form (away from the caustics):

$$w(\mathbf{x},\mathbf{v},t)=\sum_{k=1}^{N(\mathbf{x},t)}\rho_k(\mathbf{x},t)\delta(\mathbf{v}-\mathbf{u}_k(\mathbf{x},t))\,, \tag{11}$$

where each pair of $\rho_k,\mathbf{u}_k$ solves the pressureless gas equations (10).

In [34], the ansatz (11) was used to obtain a moment system satisfied by a N-phase solution for some fixed $N\in\mathbb{N}$. For example, in one space dimension and with (11), the moments are

$$m_l=\int_{\mathbb{R}}w(x,v,t)v^l dv=\sum_{k=1}^{N}\rho_k u_k^l,\qquad l=0,1,\cdots,2N. \tag{12}$$

[1]which does not match the Crandall-Lions' one as shown in [47].

The first $2N$ one-dimensional moment equations obtained by integration in v from (7) are

$$\left\{\begin{array}{rcl} \partial_t m_0 + \partial_x m_1 &=& 0, \\ \partial_t m_1 + \partial_x m_2 &=& -m_0\ \partial_x V, \\ \cdots\cdots\cdots & & \\ \partial_t m_{2N-1} + \partial_x m_{2N} &=& -(2N-1) m_{2N-2}\ \partial_x V. \end{array}\right. \tag{13}$$

It was proved in [34] that the mapping from $m_0, \cdots, m_{2N-1}$ to $\rho_1, u_1, \cdots, \rho_N, u_N$ is one-to-one, under the condition that ρ_k's are positive and u_k's are distinct, which holds for a truly N-phase solution. Hence one can express (ρ_k, u_k), $k = 1, \cdots, N$ in terms of $m_0, \cdots, m_{2N-1}$, and apply it to (12) to close the moment system with

$$m_{2N} = F_N(m_0, m_1, \cdots, m_{2N-1})\,, \tag{14}$$

for some function F_N. Thus the Liouville equation has been closed *exactly* since N is finite. When $N \leq 5$ one can find analytic expression for F_N [37]. For $N > 5$ one needs a numerical algorithm to generate F_N: see [34] for details.

We will refer to the moment system (13)-(14) as the *δ-system.*

For $N = 2$, the moment system (13)-(14) reads:

$$\left\{\begin{array}{rcl} \partial_t m_0 + \partial_x m_1 &=& 0, \\ \partial_t m_1 + \partial_x m_2 &=& -m_0\ \partial_x V, \\ \partial_t m_2 + \partial_x m_3 &=& -2m_1\ \partial_x V, \\ \partial_t m_3 + \partial_x m_4 &=& -3m_2\ \partial_x V, \end{array}\right. \tag{15}$$

with

$$m_4 = \left\{\begin{array}{ll} \frac{m_3^2 m_0 - 2m_1 m_2 m_3 + m_2^3}{m_0 m_2 - m_1^2}, & \text{if} \quad m_0 m_2 - m_1^2 \neq 0; \\ \frac{m_2^2}{m_0}, & \text{Otherwise.} \end{array}\right. \tag{16}$$

Since $m_0 m_2 - m_1^2 = \rho_1 \rho_2 (u_1 - u_2)^2$ in the case $N \leq 2$, a discontinuous flux m_4 is introduced to represent a double phase and a single phase respectively. In the case of a single phase, the definition of m_4 makes the two-phase equations equivalent to the single phase system–the pressureless gas system. In addition, in this system, the density m_0 is always positive, thus one does not face the vacuum problem.

A numerically more convenient form of the above system can be written as

$$\partial_t \mathbf{m} + \partial_x (A(p,q)\mathbf{m}) = B(\mathbf{m}), \tag{17}$$

where

$$A(p,q) = \begin{pmatrix} 0 & 1 & 0 & 0 \\ -q & p & 0 & 0 \\ 0 & -q & p & 0 \\ 0 & 0 & -q & p \end{pmatrix},$$

and

$$B(\mathbf{m}) = -\partial_x V (0, m_0, 2m_1, 3m_2)^T\,,$$

with p, q defined as

$$p = \left\{\begin{array}{ll} \frac{m_3 m_0 - m_1 m_2}{m_0 m_2 - m_1^2} \quad (= u_1 + u_2), & \text{if } m_0 m_2 - m_1^2 \neq 0; \\ 2\frac{m_1}{m_0}, & \text{Otherwise,} \end{array}\right. \tag{18}$$

and

$$q = \begin{cases} \frac{m_1 m_3 - m_2^2}{m_0 m_2 - m_1^2} \quad (= u_1 u_2), & \text{if } m_0 m_2 - m_1^2 \neq 0; \\ 0, & \text{Otherwise.} \end{cases} \tag{19}$$

Similarly for $N = 3$, one can define,

$$\begin{aligned} p_1 &= u_1 + u_2 + u_3 \\ &= \frac{m_5 m_1^2 - m_5 m_2 m_0 + m_4 m_3 m_0 - m_4 m_1 m_2 + m_3 m_2^2 - m_1 m_3^2}{m_4 m_1^2 - m_4 m_2 m_0 + m_3^2 m_0 - 2 m_1 m_2 m_3 + m_2^3}, \\ p_2 &= u_1 u_2 + u_1 u_3 + u_2 u_3 \\ &= -\frac{m_5 m_3 m_0 - m_5 m_2 m_1 + m_4 m_2^2 - m_4^2 m_0 + m_4 m_3 m_1 - m_2 m_3^2}{m_4 m_1^2 - m_4 m_2 m_0 + m_3^2 m_0 - 2 m_1 m_2 m_3 + m_2^3}, \\ p_3 &= u_1 u_2 u_3 \\ &= -\frac{m_5 m_1 m_3 - m_5 m_2^2 - m_4^2 m_1 + 2 m_4 m_3 m_2 - m_4^2 m_1 - m_3^3}{m_4 m_1^2 - m_4 m_2 m_0 + m_3^2 m_0 - 2 m_1 m_2 m_3 + m_2^3}. \end{aligned}$$

Then the δ-system takes a similar form

$$\partial_t \mathbf{m} + \partial_x (A(p_1, p_2, p_3)\mathbf{m}) = B(\mathbf{m}), \tag{20}$$

with

$$B(\mathbf{m}) = -\partial_x V(0, m_0, 2m_1, 3m_2, 4m_3, 5m_4)^T,$$

and

$$A(p_1, p_2, p_3) = \begin{pmatrix} 0 & 1 & 0 & 0 & 0 & 0 \\ 0 & 0 & 1 & 0 & 0 & 0 \\ p_3 & -p_2 & p_1 & 0 & 0 & 0 \\ 0 & p_3 & -p_2 & p_1 & 0 & 0 \\ 0 & 0 & p_3 & -p_2 & p_1 & 0 \\ 0 & 0 & 0 & p_3 & -p_2 & p_1 \end{pmatrix}.$$

To identify the number of phases, one can use the indicator functions,

$$\begin{aligned} \phi_1 &= m_0 m_2 - m_1^2, \\ \phi_2 &= m_4 m_1^2 - m_4 m_2 m_0 + m_3^2 m_0 - 2 m_1 m_2 m_3 + m_2^3, \end{aligned} \tag{21}$$

which are the denominators of p_i. If ϕ_2 is negative, then $N \geq 3$. Similarly, if $\phi_1 > 0$, $N \geq 2$. Otherwise, $N = 1$. One can easily verify that in the single phase domain (when $\phi_2 > 0, \phi_1 \leq 0$), the system will be reduced to the (single phase) pressureless gas equations. In the double phase case (when $\phi_2 > 0, \phi_1 > 0$), the triple phase system reduces to that of the double phase (17). Thus the triple phase system is valid for single, double and triple phases.

For a general problem, one first gives an *a priori* estimate on N. In one dimension such an estimate was given in [34]. In multi-d this is not so easy and one needs some physical intuition or numerical experiments to begin with. Once N is determined, one solves the N-phase system, which is valid for all n-phase situations with $n \leq N$.

2.2. **Bicharacteristic curves and their inverse mappings.** Introducing the Hamiltonian flow for the Liouville equation (7)

$$\begin{cases} \mathbf{x}'(t) = \mathbf{v}, \quad \mathbf{x}(0) = \mathbf{x}_0, \\ \mathbf{v}'(t) = -\nabla V(\mathbf{x}), \ \mathbf{v}(0) = \mathbf{v}_0. \end{cases} \tag{22}$$

The curves $(\mathbf{x}, \mathbf{v})$ are usually referred to as the *bicharacteristics* in the phase space. They generate for $t \in \mathbb{R}^+$ a Lagrangian manifold which can be understood as the

geometric solution to the eikonal equation (3) and describe the classical behavior of the solution to (10). In this case, S is the *action* associated to the Hamiltonian $\mathcal{H}(\mathbf{x},\mathbf{p}) = \frac{1}{2}\mathbf{p}^2 + V(\mathbf{x})$, with $\mathbf{p}$ being the momentum. Their projection onto the physical space with $\mathbf{v}_0 = \nabla S_0$ gives the characteristic curves (the *rays*) of the field-driven Burger's equation for the velocity:

$$\partial_t \mathbf{u} + \nabla\Big(\frac{1}{2}|\mathbf{u}|^2 + V(\mathbf{x})\Big) = 0, \qquad \mathbf{u}(x,0) = \nabla S_0. \tag{23}$$

It matches also the momentum equation of the pressureless gas equation (10) in the case when its solution is smooth.

Let $(\mathbf{x}_0(\mathbf{x},\mathbf{v},t), \mathbf{v}_0(\mathbf{x},\mathbf{v},t))$ denote the inverse mapping of the bicharacteristic curves. We emphasize that it is an unambiguous object as a consequence of Cauchy-Lipschitz's theorem for (22). Since the solution of the Liouville equation (7) is a constant along the bicharacteristic curves defined by (22), one has

$$w(\mathbf{x},\mathbf{v},t) = w\Big(\mathbf{x}_0(\mathbf{x},\mathbf{v},t), \mathbf{v}_0(\mathbf{x},\mathbf{v},t), 0\Big). \tag{24}$$

Define another mapping $\mathbb{R}^n \to \mathbb{R}^n$ by

$$\Phi_{\mathbf{x}t}(\mathbf{v}) = \mathbf{v}_0(\mathbf{x},\mathbf{v},t) - \mathbf{u}_0(\mathbf{x}_0(\mathbf{x},\mathbf{v},t)). \tag{25}$$

The zeroes of $\Phi_{\mathbf{x}t}(\mathbf{v})$ give the velocities in (11), $\{\mathbf{u}_k(x,t), k = 1,2,\cdots,N\}$ and the expression of the intensity $\rho = m_0$ reads,

$$\rho(\mathbf{x},t) = \sum_{k=1}^{N} \rho_k(\mathbf{x},t) = \sum_{k=1}^{N} \frac{\rho_0(\mathbf{x}_0(\mathbf{x},\mathbf{u}_k(\mathbf{x},t),t))}{|\frac{\partial \Phi_{\mathbf{x}t}}{\partial \mathbf{v}}|(\mathbf{u}_k(\mathbf{x},t))}. \tag{26}$$

One novelty in this paper will be to use this exact formula for the numerical computations of the intensities ρ_k, when using the forthcoming Brenier-Corrias' formulation. This improves the numerical results in the sense that much coarser grids can be used in comparison with [26, 27].

2.3. **The Heaviside closure by Brenier-Corrias.** In this subsection, we recall the construction of nonnegative 'multibranch solutions' to (23) in one space dimension through the kinetic formulation proposed in [12] (see also [11]). Let $K \in \mathbb{N}$. Consider a set of test-functions,

$$\Theta_K := \Big\{\theta \in C^0(\mathbb{R}); \qquad \partial_v^K \theta(v) \geq 0 \qquad (\mathcal{D}')\Big\},$$

together with bounded compactly supported kinetic densities:

$$\mathcal{F}_{L>0} := \Big\{f \in L^\infty, \quad 0 \leq f \leq 1 \text{ a.e. with } Supp_v(f) \subset [0,L]\Big\}.$$

Each $f \in \mathcal{F}_L$ induces a moment vector $\vec{m}(f) \in \mathbb{R}^K$ whose components read:

$$m_k(f) = \int_{\mathbb{R}^+} v^k f(v) dv, \qquad k = 0,\ldots,K-1. \tag{27}$$

It is therefore possible to define the set of 'realizable moments'

$$\mathbf{M}_K^L = \Big\{\vec{m} \in \mathbb{R}^K; \exists f \in \mathcal{F}_L \text{ such that } \vec{m} = \vec{m}(f)\Big\},$$

onto which one treats the following minimization problem:

$$\mathbf{J}_K^\theta(\vec{m}) = \inf_{f \in \mathcal{F}_L} \left\{ \int_{\mathbb{R}^+} \theta(v) f(v) dv \text{ where } \vec{m}(f) = \vec{m} \in \mathbf{M}_K^L \text{ and } \theta \in \Theta_K \right\}.$$

For any $\vec{m} \in \mathbf{M}_K^L$, there exists a unique solution to this problem which is called the *K-branch Maxwellian*: it is independent of $\theta \in \Theta_K$ and reads

$$\mathcal{M}_{K,\vec{m}}(u_1,\dots,u_K,v) = \sum_{k=1}^{K}(-1)^{k-1}H(u_k - v), \qquad u_k > u_{k+1} \geq 0, \tag{28}$$

with H standing for the Heaviside function. Thus we can consider the following map $\vec{m} : [0,L]^K \longrightarrow \mathbf{M}_K^L$:

$$m_j(u_1,\dots,u_K) := \frac{1}{1+j}\sum_{k=1}^{K}(-1)^{k-1}(u_k)^{1+j}, \qquad j = 0,\dots,K-1, \tag{29}$$

and $\vec{m}$ realizes an one-to-one C^∞ correspondence as long as $u_k > u_{k+1}$, $k \leq K$.

Definition 1. *We call K-multivalued solution any measurable function $f(x,v,t) \in \{0,1\}$ on $\mathbb{R}\times\mathbb{R}^+\times\mathbb{R}^+$ satisfying the following Vlasov equation in the sense of distributions*

$$\partial_t f + v\partial_x f - \partial_x V \partial_v f = (-1)^{K-1}\partial_v^K \tilde{m}, \qquad f(t,x,v) = \mathcal{M}_{K,\vec{m}(f)}, \tag{30}$$

where $\tilde{m}$ is a nonnegative Radon measure on $\mathbb{R}\times\mathbb{R}^+\times\mathbb{R}^+$.

Existence results for these K-multivalued solutions are provided in [12] by means of BGK approximations. Hence one establishes an equivalence between these K-multivalued solutions and the hyperbolic system of the 'realizable moments'.

Proposition 1. *(Brenier & Corrias,* [12]*)*
A measurable function $\mathcal{F}_{L>0} \ni f(t,x,v) = \sum_{k=1}^{K}(-1)^{k-1}H\big(u_k(x,t) - v\big)$ is a K-multivalued solution in the sense of Def. 1 if and only if the following entropy inequalities hold in $\mathcal{D}'(\mathbb{R}^+\times\mathbb{R})$ for all $\theta \in \Theta_K$:

$$\partial_t \int_{\mathbb{R}^+}\theta(v)f(v).dv + \partial_x \int_{\mathbb{R}^+} v\theta(v)f(v).dv + \partial_x V \int_{\mathbb{R}^+}\theta'(v)f(v).dv \leq 0. \tag{31}$$

Equality holds in case $\partial_v^K\theta(v) \equiv 0$.

The moment system coming out of the kinetic formulation (30), (28) has only $K = N$ equations and governs the evolution of velocities u_k:

$$\left\{\begin{array}{rcl} \partial_t m_0 + \partial_x m_1 &=& 0, \\ \partial_t m_1 + \partial_x m_2 &=& -m_0\ \partial_x V, \\ \cdots\cdots\cdots & & \\ \partial_t m_{K-1} + \partial_x m_K &=& -(K-1)m_{K-2}\ \partial_x V, \end{array}\right. \tag{32}$$

in which,

$$m_j = \int_{\mathbb{R}^+} f(x,v,t)v^j dv, \quad j = 0,1,\cdots,K.$$

Once again, closing it amounts to finding a nonlinear function such that:

$$m_K = \tilde{F}_K(m_0,m_1,\cdots,m_{K-1}). \tag{33}$$

Their expression is generally involved. For $K < 5$, it is available in [47]. To obtain the density, it was proposed in [26, 27] to solve the linear conservation equation

$$\partial_t \rho_k + \partial_x(u_k\rho_k) = 0, \qquad \text{for } k = 1,\cdots,N\,. \tag{34}$$

We refer to the moment system (32)-(33) as the *H-system*.

The H-system for $K = 2$ reads

$$\left\{ \begin{array}{rcl} \partial_t m_0 + \partial_x m_1 & = & 0, \\ \partial_t m_1 + \partial_x m_2 & = & -m_0\, \partial_x V, \end{array} \right. \tag{35}$$

where the relations between the moments m_k's and Riemann coordinates u_k's are

$$m_0 = u_1 - u_2, \qquad m_1 = \frac{1}{2}\Big((u_1)^2 - (u_2)^2\Big).$$

This can obviously be inverted,

$$u_1 = \frac{m_1}{m_0} + \frac{m_0}{2}, \qquad u_2 = \frac{m_1}{m_0} - \frac{m_0}{2},$$

which implies that:

$$m_2 = \frac{1}{3}\Big((u_1)^3 - (u_2)^3\Big) = \tilde{F}_2(m_0, m_1) = \frac{(m_1)^2}{m_0} + \frac{(m_0)^3}{12}.$$

Hence the mapping $m_0, m_1 \mapsto \tilde{F}_2(m_0, m_1)$ is continuous across a phase boundary. In this simple case, u_1, u_2 are solutions of an invertible linear algebraic system. For $K = 3$, following [47],

$$u_2 = \frac{(m_0)^3 + 6m_2 - 6m_0 m_1}{3\big((m_0)^2 + 2m_1\big)}; \qquad u_{1,3} = \frac{-4\big((m_0)^3 - 3m_2\big) \pm \sqrt{\Delta}}{12\big((m_0)^2 + 2m_1\big)}$$

together with:

$$\Delta = 16\big((m_0)^3 - 3m_2\big)^2 - 24\big((m_0)^2 + 2m_1\big)\big((m_0)^4 + 12(m_1)^2 - 12m_2 m_0\big).$$

One can write $m_3 = \tilde{F}_3(m_0, m_1, m_2) = \frac{1}{4}\big((u_1)^4 - (u_2)^4 + (u_3)^4\big)$ in terms of m_0, m_1, m_2 to close the system

$$\left\{ \begin{array}{rcl} \partial_t m_0 + \partial_x m_1 & = & 0, \\ \partial_t m_1 + \partial_x m_2 & = & -m_0\, \partial_x V, \\ \partial_t m_2 + \partial_x m_3 & = & -2m_1\, \partial_x V. \end{array} \right. \tag{36}$$

When one is led to use for instance the double phase system (35) in a single phase domain (where $u_1 = u_2$), the moments $m_{1,2} \equiv 0$ and this corresponds to the vacuum for the Euler equations. This is the reason why, as in [26, 47], we shall use initial data for which a single phase is split into slightly different ones by means of a small parameter (see §5.1 for instance). This stabilizes also their numerical processing since it brings back the system inside a strict hyperbolicity region as its characteristic velocities are given by the u_k's.

Uniqueness results for both (32) and (13) are very sparse: see [39, 29, 8] in the case $K = N = 1$, [51] for $K = 2$ and [1, 7, 23, 26] for $K > 2$ in the strictly hyperbolic case and $\partial_x V \in L^1 \cap L^\infty(\mathbb{R})$.

3. Some analytical properties of the 1-D moment equations

Let us point out differences between the two moment systems.

- The H-system is a non-strictly rich 1D hyperbolic system whereas the δ-system is only weakly hyperbolic.
- The H-system decouples the computation of velocity u_k from the intensity (defined by (34)), but the δ-system couples the computation of these quantities.

- The H-system is a mathematical formulation without too much physical meaning while the δ-system arises from a rigorous Wigner analysis for the semiclassical limit of the Schrödinger equation.

Next we explore some common features of both moment systems.

3.1. **Propagation of the phase boundaries.** First, we characterize the nature of the phase boundaries and study their propagations. As an example, we study the phase boundary from a single phase to triple phases. The transition properties in other circumstances is similar.

Lemma 1. *Assume $K = N = 3$ and let $(\bar{x}, t)$ be a phase boundary separating a triple phase region on the left from a single phase one on the right. Assume*
- *$\rho_3(.,t)$, $u_3(.,t)$ are continuous at $\bar{x}$,*
- *$\rho_1(x,t) = \rho_2(x,t) = 0$ and $u_1(x,t) = u_2(x,t) = u_3(x,t)$ for $x > \bar{x}$,*
- *$u_1(\bar{x}-,t) = u_2(\bar{x}-,t)$,*

as shown in Fig 1 then its characteristic speed is $\sigma = u_2(\bar{x}-,t)$ for both moment systems (20) and (36).

If a discontinuity at $(\bar{x},t)$ separates a single phase region on the left from a triple phase one on the right, then under similar assumptions, the speed of the phase boundary is $\sigma = u_2(\bar{x}+,t)$.

Proof. It is merely a consequence of the classical Rankine-Hugoniot conditions. We perform the computation first for the H-system (36). From (29), we deduce that

$$m_0 = u_1 - u_2 + u_3, \qquad m_1 = \frac{1}{2}\Big((u_1)^2 - (u_2)^2 + (u_3)^2\Big).$$

Hence the hypotheses of Lemma 1 imply: ($[\cdot]$ standing for the jump of a quantity)

$$\sigma = \frac{1}{2}\frac{\big[(u_1)^2 - (u_2)^2\big]}{\big[u_1 - u_2\big]} = \frac{1}{2}\big(u_1(\bar{x}-,t) + u_2(\bar{x}-,t)\big) = u_2(\bar{x}-,t).$$

Concerning the δ-system (20), we recall from the moments' expression (12) that,

$$m_0(\bar{x}-,t) = \rho_1 + \rho_2 + \rho_3, \quad m_0(\bar{x}+,t) = \rho_3.$$

$$m_1(\bar{x}-,t) = \rho_1 u_1 + \rho_2 u_2 + \rho_3 u_3, \quad m_1(\bar{x}+,t) = \rho_3 u_3.$$

This clearly leads to:

$$\sigma = \frac{\big[m_1\big]}{\big[m_0\big]} = u_2(\bar{x}-,t)$$

□

Such discontinuities across which the phase number $N(x,t)$ changes are *under-compressive shocks* since the characteristics from one side are parallel to the shock, while from the other side they impinge into it. Thus they do not satisfy the strict Lax inequalities.

3.2. **Equivalence of weak solutions with enough moments.** We now aim at establishing the equivalence of the two moment systems (13) and (32) when a large enough number of moments is involved.

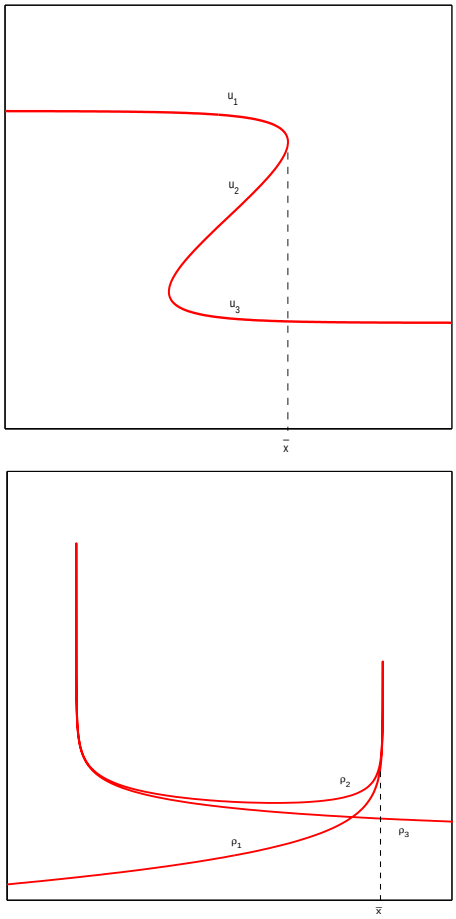

FIGURE 1. Illustration of the case considered in Lemma1.

Theorem 1. *Let $K = N \in \mathbb{N}$ be fixed, $0 \leq \rho_0$ and u_0 be a given smooth function, $f^{(1)}(x,v,t)$ a solution to the Liouville equation (7) with initial condition, $f^{(1)}(x,v,0) = H(v-u_0(x))$. Consider the set:*

$$\mathcal{C} = \Big\{ v \in \mathbb{R}^+ \text{ such that } f^{(1)}(x,v,t) = 1,\ f^{(1)}(x,v,0) = H(v-u_0(x)) \Big\}.$$

Assume that it has only M connected components. If
– $M = \frac{1}{2}(K+1)$ (K odd) or $M = K/2$ (K even),
– $N = K$ in (13),
then the δ-system (13) and the H-system (32)–(26) produce the same weak solution (ρ_k, u_k), $k = 1, ..., N$.

Proof. From Theorem 3.5 in [12], we know that the singular source term $\tilde{m}$ in (30) is null under our assumptions which guarantee that the number of moments involved is big enough. Then both moment systems (13) and (32) are obtained by integration in v of the following Liouville equation (see (7) and (30)):

$$\partial_t w + v\partial_x w - V'(x)\partial_v w = 0, \tag{37}$$

with two different initial data:

$$w^{(1)}(x,v,0)=\rho_0(x)\delta(v-u_0(x)),\quad w^{(2)}(x,v,0)=H(u_0(x)-v).$$

Using the bicharacteristic curves defined in (22) one gets the exact solution of (37),

$$w(x,v,t)=w(x_0(x,v,t),v_0(x,v,t),0).$$

In particular with the above initial conditions, we have,

$$w^{(1)}(x,v,t)=\rho_0(x_0(x,v,t))\delta(\Phi_{xt}(v)),\quad w^{(2)}(x,v,t)=H(-\Phi_{xt}(v)),$$

with $\Phi_{xt}(v)$ defined in (25). Corresponding to $w^{(1)}$, velocities $\{u_k^{(1)},k=1,\cdots,N\}$ are the zeroes of $\Phi_{xt}(v)$, so are the velocities corresponding to $w^{(2)}$. So both system yield the same velocities. For the H-system, if one uses the formula, (see (26))

$$\rho_k(x,t)=\frac{\rho_0(x_0(x,u_k,t))}{|\Phi'_{xt}(u_k)|},\quad k=1,2,\cdots,N,$$

then the two systems produce the same density solutions as well. □

If we do not use enough moments, these two moment systems generate different 'viscosity' solutions by introducing different cuts (shocks) across the underrepresented phases: see numerical experiments in Section 5.

4. Numerical discretizations of the moment systems

We shall consider from now on a Cartesian computational grid determined by the positive parameters Δx, Δt which stand respectively for the uniform mesh size and the time step. Accordingly we will denote $x_j=j\Delta x$ and $t_n=n\Delta t$.

4.1. Kinetic schemes for the δ-system: $\partial_x V\equiv 0$.

Kinetic schemes were used in [34] to solve the moment system. It has been shown in [34, 9] that kinetic schemes are best suited for such weakly hyperbolic equations of the pressureless gas type when considering both their accuracy and their robustness in treating the vacuum. Let us first consider the case with a constant potential,

$$\partial_t w+v\partial_x w=0, \tag{38}$$

for which the exact solution, within one time step, is given by

$$w(x,v,t)=w(x-v(t-t^n),v,t_n).$$

Using the ansatz (11) with $N(x,t)=N\in\mathbb{N}$,

$$w(x,v,t)=\sum_{k=1}^{N}\rho_k(x,t)\delta\Big(v-u_k(x,t)\Big),$$

one integrates (38) over $(x_{j-1/2},x_{j+1/2})\times\mathbb{R}_v\times(t_n,t_{n+1})$ and gets,

$$(m_l)_{n+1,j}-(m_l)_{n,j}+\frac{\Delta t}{\Delta x}\Big(f^{(l)}_{n,j+\frac12}-f^{(l)}_{n,j-\frac12}\Big)=0, \tag{39}$$

where, for $l=0,...,2N-1$,

(40)

$$(m_l)_{n,j}=\int_{x_{j-\frac12}}^{x_{j+\frac12}}\frac{m_l(x,t_n)}{\Delta x}dx,\qquad f^{(l)}_{n,j+\frac12}=\frac{1}{\Delta t}\int_0^{\Delta t}\int_{\mathbb{R}}w(x_{j+\frac12}-vt,v,t_n)v^l dv.$$

The first order scheme given by (40) corresponds to a flux-splitting,

$$f^{(l)}_{n,j+\frac{1}{2}} = \sum_{k=1}^{N} (\rho_k u_k^{l-1} u_k^+)_{n,j} + (\rho_k u_k^{l-1} u_k^-)_{n,j+1}. \tag{41}$$

Here we have used the conventional notations

$$u^+ = \frac{1}{2}(|u| + u), \qquad u^- = -\frac{1}{2}(|u| - u).$$

One can use a piecewise linear construction for (ρ_k, u_k) to obtain a formally second order scheme (the indices k, n are dropped for convenience),

$$\left\{ \begin{array}{lcll} \rho(x) & = & \rho_j + D\rho_j (x - x_j), & \\ u(x) & = & \overline{u}_j + Du_j (x - x_j), & \end{array} \right. \qquad \text{for} \quad x_{j-1/2} < x < x_{j+1/2}, \tag{42}$$

where $\overline{u}_j$ is chosen as

$$\overline{u}_j = u_j - \frac{D\rho_j Du_j}{12\rho_j} \Delta x^2, \tag{43}$$

in order to have the conservation property. Namely, the cell average of $q_j(x) = \rho_j(x) u_j(x)$ must be $q_j = \frac{1}{\Delta x} \int_{x_j - \frac{1}{2}}^{x_{j+\frac{1}{2}}} \rho(x) u(x) dx$. After some calculation, one gets

$$f^{(l)}_{j+\frac{1}{2}} = \sum_{k=1}^{N} \frac{1}{\Delta t} \int_{x^L_{j+\frac{1}{2}}}^{x_{j+\frac{1}{2}}} \rho_k(x) u_k(x)^{l-1} dx - \frac{1}{\Delta t} \int_{x_{j+\frac{1}{2}}}^{x^R_{j+\frac{1}{2}}} \rho_k(x) u_k(x)^{l-1} dx, \tag{44}$$

where

$$x^L_{j+1/2} = x_{j+1/2} - \Delta t \frac{(\overline{u}_j + \frac{\Delta x}{2} Du_j)^+}{1 + \Delta t Du_j}, \; x^R_{j+1/2} = x_{j+1/2} + \Delta t \frac{(\overline{u}_{j+1} - \frac{\Delta x}{2} Du_{j+1})^-}{1 + \Delta t Du_{j+1}}. \tag{45}$$

The numerical flux can be written in explicit form,

$$\begin{aligned} f^{(l)}_{j+\frac{1}{2}} \;=\; & \sum_{s=0}^{l-1} C^s_{l-1} (u_k)^s_j (Du_k)^{l-s-1}_j \Big[\frac{1}{(l-s)\Delta t} (\rho_k)_j \big((\tfrac{1}{2}\Delta x)^{l-s} - (x^L_{j+\frac{1}{2}} - x_j)^{l-s} \big) \\ & \qquad + \frac{1}{(l-s+1)\Delta t} (D\rho_k)_j \big((\tfrac{1}{2}\Delta x)^{l-s+1} - (x^L_{j+\frac{1}{2}} - x_j)^{l-s+1} \big) \Big] \\ + \; & \sum_{s=0}^{l-1} C^s_{l-1} (u_k)^s_{j+1} (Du_k)^{l-s-1}_{j+1} \Big[\frac{1}{(l-s)\Delta t} (\rho_k)_{j+1} \big((x^R_{j+\frac{1}{2}} - x_{j+1})^{l-s} - (-\tfrac{1}{2}\Delta x)^{l-s} \big) \\ & \qquad + \frac{1}{(l-s+1)\Delta t} (D\rho_k)_{j+1} \big((x^R_{j+\frac{1}{2}} - x_{j+1})^{l-s+1} - (-\tfrac{1}{2}\Delta x)^{l-s+1} \big) \Big] \end{aligned}$$

The slope limiters are chosen as follows,

$$\begin{aligned} D\rho_j &= \frac{1}{2} \Big(\operatorname{sgn}(\rho_{j+1} - \rho_j) + \operatorname{sgn}(\rho_j - \rho_{j-1}) \Big) \\ &\qquad \times \min \left\{ \frac{|\rho_{j+1} - \rho_j|}{\Delta x}, \frac{|\rho_j - \rho_{j-1}|}{\Delta x}, \frac{2\rho_j}{\Delta x} \right\}, \\ Du_j &= \frac{1}{2} \Big(\operatorname{sgn}(u_{j+1} - u_j) + \operatorname{sgn}(u_j - u_{j-1}) \Big) \\ &\qquad \times \min \left\{ \frac{|u_{j+1} - u_j|}{(1 - \Delta x D\rho_j / 6\rho_j)\Delta x}, \frac{|u_j - u_{j-1}|}{(1 + \Delta x D\rho_j / 6\rho_j)\Delta x}, \frac{1}{\Delta t} \right\}. \end{aligned} \tag{46}$$

It is chosen so as to ensure several important properties (see [9]) such as the positivity of the intensity and the maximum principles on the velocities u_k.

In the numerical implementation, given ρ_k, u_k, the indicator functions (21) are computed first to detect the number of phases. We then utilize the scheme (39) to update the moments. The multivalued intensity and velocity can be recovered from these moments as described in section 2.4. For all the numerical tests presented in this paper, we take $N \leq 3$. In the single phase region, we take,

$$\rho_1 = m_0, \quad \rho_2 = \rho_3 = 0, \quad u_1 = u_2 = u_3 = u = \frac{m_1}{m_0}.$$

4.2. **A kinetic scheme for varying potential: $\partial_x V \neq 0$.** Several numerical methods for hyperbolic systems with geometrical source terms have been recently proposed. These schemes are *well-balanced* in the sense that smooth steady-state solutions are preserved numerically either exactly or with at least a second order accuracy [14, 30, 25, 33, 45]. Indeed, the δ-system (13) admits steady solutions,

$$\rho_k \geq 0, \ \rho_k u_k = C_k, \ \frac{u_k^2}{2} + V(x) = D_k, \quad k = 1, 2, \cdots, N, \tag{47}$$

in which C_k and D_k are constants.

In this section, we will follow mostly the method proposed by Perthame and Simeoni [45] which relies on energy balancing at the microscopic level. Namely, particles from adjacent cells can cross the interfaces as long as their kinetic energy is big enough to overcome the potential jump. Otherwise they will be reflected backwards[2] (their velocity will change sign). This idea gives rise to the following scheme for the kinetic equation,

$$w_{n+1,j} = w_{n,j} - \frac{\Delta t}{\Delta x} v \left(w^-_{n,j+\frac{1}{2}} - w^+_{n,j-\frac{1}{2}} \right),$$

where the one-sided numerical fluxes are given by:

$$\begin{aligned} w^-_{n,j+\frac{1}{2}}(v) &= w_{n,j}(v)\, \mathbf{1}_{\{v>0\}} + w_{n,j}(-v)\, \mathbf{1}_{\{v<0\}\cap\{v^2\leq 2\Delta V_{j+\frac{1}{2}}\}} \\ &\quad + w_{n,j+1}\big(- \sqrt{v^2 - 2\Delta V_{j+\frac{1}{2}}}\big)\, \mathbf{1}_{\{v<0\}\cap\{v^2>2\Delta V_{j+\frac{1}{2}}\}}, \end{aligned}$$

and

$$\begin{aligned} w^+_{n,j-\frac{1}{2}}(v) &= w_{n,j}(v)\, \mathbf{1}_{\{v<0\}} + w_{n,j}(-v)\, \mathbf{1}_{\{v>0\}\cap\{v^2\leq -\Delta V_{j-\frac{1}{2}}\}} \\ &\quad + w_{n,j-1}\big(\sqrt{v^2 + 2\Delta V_{j-\frac{1}{2}}}\big)\, \mathbf{1}_{\{v>0\}\cap\{v^2>-\Delta V_{j-\frac{1}{2}}\}}, \end{aligned}$$

with

$$\forall j \in \mathbb{Z}, \qquad \Delta V_{j+\frac{1}{2}} = V_{j+1} - V_j.$$

Integrating with respect to v, one immediately obtains a 'conservative' scheme in the physical space,

$$(m_l)_{n+1,j} = (m_l)_{n,j} - \frac{\Delta t}{\Delta x}\Big(f^{-(l)}_{n,j+\frac{1}{2}} - f^{+(l)}_{n,j-\frac{1}{2}} \Big), \qquad l = 0, ..., 2N-1, \tag{48}$$

[2]There is no "tunnel effect" anymore at this scale.

with the numerical fluxes, (we drop the n index for clarity)

$$\begin{aligned} f^{-(l)}_{n,j+\frac12} &= \int_{\mathbb{R}} w^-_{j+\frac12} v^l dv \\ &= \sum_{k=1}^N (\rho_k)_j (u_k)_j^l \, \mathbf{1}_{\{(u_k)_j>0\}} + (\rho_k)_j (-(u_k)_j)^l \, \mathbf{1}_{\{(u_k)_j>0\}\cap\{(u_k)_j^2\le 2\Delta V_{j+\frac12}\}} \\ &\quad + (\rho_k)_{j+1}(u_k)_{j+1}\big(-\sqrt{(u_k)_{j+1}^2 + 2\Delta V_{j+\frac12}}\big)^{l-1} \mathbf{1}_{\{(u_k)_{j+1}<0\}\cap\{(u_k)_{j+1}^2>-2\Delta V_{j+\frac12}\}}, \end{aligned}$$

and

$$\begin{aligned} f^{+(l)}_{n,j-\frac12} &= \int_{\mathbb{R}} w^+_{j-\frac12} v^l dv \\ &= \sum_{k=1}^N (\rho_k)_j (u_k)_j^l \, \mathbf{1}_{\{(u_k)_j<0\}} + (\rho_k)_j (-(u_k)_j)^l \, \mathbf{1}_{\{(u_k)_j<0\}\cap\{(u_k)_j^2\le -2\Delta V_{j-\frac12}\}} \\ &\quad + (\rho_k)_{j-1}(u_k)_{j-1}\big(\sqrt{(u_k)_{j-1}^2 - 2\Delta V_{j-\frac12}}\big)^{l-1} \mathbf{1}_{\{(u_k)_{j-1}>0\}\cap\{(u_k)_{j-1}^2>2\Delta V_{j-\frac12}\}}. \end{aligned}$$

If $\partial_x V \equiv 0$, one can verify that this numerical scheme reduces to the one given in the previous section. So far this method has not been extended to second order.

4.3. **A local Lax-Friedrichs scheme for the H-system.** Discretization of the H-system (32) could be done using similar kinetic scheme starting from the homogeneous Liouville equation (33) (38). According to (28), the first-order numerical fluxes are now given by

$$\tilde f^{(l)}_{n,j+\frac12} = \frac{1}{l+1}\sum_{k=1}^K (-1)^{k-1}\Big[(u_k^l u_k^+)^n_j + (u_k^l u_k^-)^n_{j+1}\Big], \qquad l=0,...,K-1. \tag{49}$$

However a better outcome is obtained by the so-called *local Lax-Friedrichs* (LLxF for short) scheme which in the present setting reads: (compare with (49))

$$\begin{aligned} \tilde f^{(l)}_{n,j+\frac12} &= \tfrac{1}{2(l+1)}\textstyle\sum_{k=1}^K (-1)^{k-1}\Big[(u_k^{l+1})^n_j + (u_k^{l+1})^n_{j+1}\Big] \\ &\quad - \max_{k;\ j,j+1} |u_k|^n \Big((m^l)^n_{j+1} - (m^l)^n_j\Big), \end{aligned} \qquad l=0,...,K-1. \tag{50}$$

Both kinetic and LLxF discretizations are endowed with similar numerical dissipation. The main difference between them stems from the rendering of N-waves which appear for instance when bifurcating from a one-phase to a three-phases solution; see Figs. 3 and 4. Its second order extension is the *Nessyahu-Tadmor* (NT) scheme already used in [17, 26, 47]; it has the drawback of being less stable in the vicinity of non-strictly hyperbolic points. In order to compute the densities ρ_k, we shall use an approximation of the explicit formula (26). As long as $\partial_x V \equiv 0$, the Hamiltonian flow (22) can be solved exactly as:

$$v(t) = v_0, \qquad x(t) = x_0 + v_0 t = x_0 + v(t)t\,.$$

Thus characteristics $x(t)$ are straight lines along which $u_k(x(t),t)$ is constant, and

$$\Phi_{xt}(v) = v - u_0(x - vt)\,.$$

Consequently

$$\frac{\partial \Phi_{xt}(v)}{\partial v} = 1 + t u_0'(x-vt) \Rightarrow \frac{\partial \Phi_{xt}}{\partial v}\big(u_k(x,t)\big) = 1 + t u_0'\big(x - u_k(x,t)t\big).$$

Given u_k, a simple way to deduce the ρ_k's numerically follows from (26):

$$(\Phi')_j^n = 1 + t_n u_0'\big(j\Delta x - t_n (u_k)_j^n\big), \qquad (\rho_k)_j^n = \frac{\rho_0\big(x_j - t_n.(u_k)_j^n\big)}{|(\Phi')_j^n|}. \tag{51}$$

In the case of a nonconstant smooth potential $V(x)$, one observes simply that the (vector of the) numerical fluxes of the LLxF scheme (50) read:

$$\tilde{f}_{n,j+\frac{1}{2}} = \tilde{f}\left(\vec{u}_j^n, \vec{u}_{j+1}^n\right), \qquad \mathbb{R}^K \ni \vec{u}_j^n = \left((u_k)_j^n\right)_{k=0,\dots,K-1}.$$

At this point, from [24, 26], we use the fact that any conservative flux for homogeneous conservation laws can be modified to handle source terms in a well-balanced (WB, for short) manner in the following way:

$$\vec{u}_j^{n+1} = \vec{u}_j^n - \tfrac{\Delta t}{\Delta x}\left(\tilde{f}^{WB}_{n,j+\frac{1}{2},-} - \tilde{f}^{WB}_{n,j-\frac{1}{2},+}\right);$$

$$\begin{array}{rcl} \tilde{f}^{WB}_{n,j+\frac{1}{2},-} & = & \tilde{f}\left(\vec{u}_j^n, \vec{u}^n_{j+\frac{1}{2},-}\right), \\ & \text{with} & \vec{u}^n_{j+\frac{1}{2},-} = v(x_j),\ \partial_x v(x)^2 = 2V'(x),\ v(x_{j+1}) = \vec{u}_{j+1}^n; \end{array} \tag{52}$$

$$\begin{array}{rcl} \tilde{f}^{WB}_{n,j-\frac{1}{2},+} & = & \tilde{f}\left(\vec{u}^n_{j-\frac{1}{2},+}, \vec{u}_j^n\right), \\ & \text{with} & \vec{u}^n_{j-\frac{1}{2},+} = v(x_j),\ \partial_x v(x)^2 = 2V'(x),\ v(x_{j-1}) = \vec{u}_{j-1}^n. \end{array}$$

The WB property for steady-state solutions is obvious since in this case, both $\vec{u}^n_{j+\frac{1}{2},-}$ and $\vec{u}^n_{j-\frac{1}{2},+}$ are equal to $\vec{u}_j^n$ and therefore one obtains trivially $\vec{u}_j^{n+1} = \vec{u}_j^n$. Since the steady equations read $\partial_x \vec{v}(x)^2 = 2V'(x)$, they can be solved analytically:

$$\vec{u}^n_{j-\frac{1}{2},+} = \sqrt{(\vec{u}_{j-1}^n)^2 - 2\Delta V_{j-\frac{1}{2}}}, \qquad \vec{u}^n_{j+\frac{1}{2},-} = \sqrt{(\vec{u}_{j+1}^n)^2 + 2\Delta V_{j+\frac{1}{2}}},$$

together with a convenient choice of the signs. There is however a little difficulty lying in the fact that the steady-state relations are singular for instance if $((u_k)_{j-1}^n)^2 < 2\Delta V_{j-\frac{1}{2}}$ and this corresponds to the case where particles are reflected in the kinetic interpretation of §4.2. In this case, the square roots can become complex-valued. The easiest way out is thus to replace $\tilde{f}(\vec{u}^n_{j-\frac{1}{2},+}, \vec{u}_j^n)$ with $\tilde{f}(\vec{u}_{j-1}^n, \vec{u}^n_{j-\frac{1}{2},-})$ for which the square root will surely be real-valued because $\Delta V_{j-\frac{1}{2}}$ will have the opposite sign. Deducing the intensities is done in a way similar to the homogeneous case but one needs to take into account the curvature of the characteristic curves. For moderate values of $t_n > 0$, one may approximate system (22) by the Trapezoidal rule

$$x(t^n) = x_0 + \frac{1}{2} t_n (u + u_0), \qquad u(t_n) = u_0 - \frac{1}{2} t_n \Big(V'(x_0) + V'(x(t^n))\Big),$$

and the value of x_0 can be found iteratively by the Newton's method. At this point, formula (51) can still be used. Of course, for greater values of t_n, one can (should!) iterate this recipe on convenient time intervals.

For $N = K \geq 2$, it doesn't seem possible to perform a rigorous convergence analysis even for the flux-splitting schemes (39), (41) and (49), and uniqueness results for (13) and (32), in order to relate these numerical approximations to the semiclassical limit. Therefore we plan to rely on numerical experiments to validate these approaches.

5. Numerical experiments

5.1. **A free particle model for a Gaussian pulse.** We first consider the following problem which models the evolution in time of a pulse-type signal for (1), (2) in the semiclassical limit. More precisely, for $x \in [-1,1]$, we choose $p \in \mathbb{N}$:

$$\rho_0(x) = \exp\Big(-\big(x-\frac{1}{2}\big)^2\Big),\ u_0(x) = -\sin(\pi x)|\sin(\pi x)|^{p-1}. \tag{53}$$

Intuitively, the decreasing interval of the velocity profile will eventually lead to caustics.

The mesh size and time steps are $\Delta x = \Delta t = 0.006$ respectively for all the runs (except otherwise stated) and results are shown at time $T = 1$. To approximate the H-system (36) and the δ-system (20) (both allow at most three phases to be fully rendered), we use the first order LLxF scheme (50) and the kinetic schemes ((44) and (48)) respectively. The multivalued phase functions $S(.,t_n)$ can be deduced from the $u_k(.,t_n)$ by numerical integration as in [26]. The numerical results are compared with those obtained using the ray tracing (denoted by "ray" in all figures).

One cusp caustic: p=1. In this case, the exact solution of the rays contains self-interference, develops a cusp singularity, and hence admits at most three phases. The density blows up on the caustic curve. The rays are displayed on Fig. 2. Some numerical approximations obtained with the H-system (36) with $K = 3$ are presented on Fig. 3: initial data were chosen as in [26], namely $u_1(t=0,.) = u_0 + \frac{\Delta x}{10}$, $u_2(t=0,.) = u_0$, $u_3(t=0,.) = u_0 - \frac{\Delta x}{10}$. The densities are computed based on the explicit formula (51). Meanwhile, the numerical results for the δ-system are depicted in Fig. 4.

Since the number of physical phases does not exceed the number of phases that the systems (36) and (20) support, the numerical solutions agree nicely with the exact ones, which are produced by simple ray tracing. A spurious shock in the velocity solution can be observed around the sonic point at $x = 0$ in the results of the kinetic scheme. This is due to the loss of consistency of the scheme at this point, as studied in [2, 9]. For instance in the case of single phase, if $u_j > 0$ and $u_{j+1} < 0$, then the first order kinetic scheme gives,

$$(\rho u)_{j+\frac{1}{2}} = \rho_j u_j + \rho_{j+1} u_{j+1} = 2\rho(x_{j+\frac{1}{2}}) u(x_{j+\frac{1}{2}}) + O(\Delta x).$$

This lack of consistency appears more severely in the first order kinetic scheme and becomes smaller as one uses higher order schemes.

For the delta-system (20), the numerical solution ρ_2 often displays spurious peaks [34], whereas the multivalued velocities u_1, u_2 and u_3 can usually be well produced. This is because the computation of the multivalued intensities involves inverting a matrix of the Vandermonde type, which is ill conditioned near the phase boundaries (i.e. where u_3 or u_1 get close to u_2). Therefore, we also rely on the formula (51) for the computation of ρ_2.

Meanwhile in Fig. 5, we compare the first order LLxF to solve the the delta-system and compared the numerical solutions with the ones from kinetic scheme. The result of LLxF for the δ system is not competitive compared to the kinetic scheme for the same system, while for the H-system the LLxF seems to outperform the kinetic scheme.

Two cusps merging into one: p=2. In this case, the initial data u_0 has an inflection point at $x = 0$ and two cusp singularities develop inside the geometric

solution which exhibits at most five phases. But these two singularities will eventually merge when time goes to infinity. More precisely, the size of the interval where five different values appear in u_k shrinks like[3] $O(1/t)$, see Fig. 6. Therefore it is attempting to simulate this problem with just the 3-phase closure: see the numerical results on Fig. 7 and Fig. 8 . We stress that it would be possible to reconstruct by symmetry the whole spectrum of u (but not ρ since ρ_0 doesn't admit $x = 0$ as a center of symmetry) as in [26]. Notably, the two advocated formulations provide different results: the H-closure produces better solutions, particularly for the top and the bottom branch. But the δ-closure captures the locations of the phase boundaries more accurately. We performed another run on the same configuration with a much finer grid $\Delta x = 0.0006$; one observes that in this case, the H-systems displays more accurate phases' boundaries. The results are very similar to the ones generated by the δ-system: see Fig.9.

The 'square signal': p=100. In this case, the initial data develops two cusp singularities involving five phases which stand still forever: see the rays in Fig.12. We consider this test case as a way to visualize the effects of the 'measure source terms' responsible for the closure of the Vlasov equation (7), (30) onto the geometric solution of (23) when the number of phases used in the moment system is too low. We use 3-phase systems for both closures. We used the H-system (36) with the following initializations which exploit the symmetry property of u_0:

$$u_1(t=0,.) = u_0 \mathbf{1}_{x<0} + \frac{\Delta x}{10},\ u_2(t=0,.) = u_0 \mathbf{1}_{x<0},\ u_3(t=0,.) = u_0 \mathbf{1}_{x<0} - \frac{\Delta x}{10}.$$

With the H-system involving three moments and $\Delta x = 0.006$, the numerical solutions miss completely the exact one (see top figure in Fig 11). If one refines the grid (as for $p = 2$) or exploits symmetry, as explained in [26], results are improved significantly although some discrepancy still exists because of the signals' sharpness (see bottom figure in Fig 11). The δ-system, despite of the moments' shortage, gives much better approximation. See Fig.12. Note that the two different closures again display different 'cuts' in the numerical solutions.

5.2. **The harmonic oscillator.** In the last numerical experiment, we consider the Schrödinger equation (1) with a confining potential

$$V(x) = \frac{1}{2}x^2,$$

together with the initial conditions:

$$\rho_0(x) = \exp\Big(-\big(x - \frac{1}{2}\big)^2\Big), \qquad u_0(x) = -\tanh(5x). \tag{54}$$

The exact solution can be found by the method of characteristics since the system (22) can be integrated as follows for $x_0 \in \mathbb{R}$:

$$x(t) = \cos(t)x_0 + \sin(t)u_0(x_0), \qquad u(x(t),t) = -\sin(t)x_0 + \cos(t)u_0(x_0).$$

See Fig. 13 for the rays. This corresponds to a rotation in the phase space at unitary angular speed. For δ-system, the well-balanced kinetic scheme presented in §4.2 is used and the numerical solutions at $T = 0.5$ are displayed on Fig. 15. On the other hand, the results on Fig.14 have been obtained using the H-system (52) and (51) for which no iterative algorithm is necessary since $V'(x) = x$ is linear.

[3] We have $u_0(x) = -\sin(\pi x)|\sin(\pi x)|$ and following (22), $\frac{dx}{dx_0} = 1 + t.u_0'(x_0) = 1 - t.\pi|\sin(2\pi x)|$ since $V' \equiv 0$, hence the exact size is $\frac{1}{2\pi}|\arcsin(1/t\pi)|$.

An adaptive time-step algorithm has been used in order to keep a constant CFL number around 0.95. Both numerical methods produce good results comparing to the exact ones. Since the potential is smooth, direct splitting of the moment systems (the hyperbolic part and the potential part) may also produce good results for the δ-system. In the case of the H-closure, a time-splitting approach is unstable as noted in [11]. For a discontinuous or singular potential, the well balanced schemes can achieve much better results (see for example [14, 30, 25, 33, 45]), but one then deals with *nonconservative products*, [36].

6. Conclusion

We addressed the issue of reproducing efficiently the semiclassical (WKB) limit of the linear Schrödinger equation (1)–(2) by means of a kinetic formalism involving the Vlasov equation (7) which can be closed in two ways, following either [34, 48] or [12, 26]. The former closure will generate a system of weakly hyperbolic system. This second choice produces the systems (32) which are less demanding numerically and represent an interesting alternative for 1D computations. In the multi-dimensional case, only the Dirac closure leading to (13) can be exploited [34]. Both moment systems provide Eulerian methods to compute the multivalued intensity and velocity *only* in the *physical* space. We compare analytical properties of these two moment systems, and introduce new numerical methods to solve these moment systems which have been extensively tested and compared with each other and with the solution obtained by the ray tracing. The numerical results obtained in this paper gives better results than those previously produced for similar moment systems.

We point out that solving the moment system is a delicate numerical task compared to a standard strongly hyperbolic system, even when the total number of phases is known *a priori*. The moment systems are not strongly hyperbolic, and the fluxes maybe discontinuous across the caustics. The discontinuities at which the phase number changes are *undercompressive shocks*. Each of these contributes to the numerical challenges not faced by standard shock capturing techniques. Although the numerical results we obtained are more reasonable than the previous efforts, they are still not very satisfactory when judged by the modern standard of shock capturing for strongly hyperbolic systems. More investigations and better methods seem to be needed in this exploration.

The applications of the moment methods are not restricted to the computation of the semiclassical limits of the Schrödinger equation. Similar problems arise in geometric optics [17, 47], seismic imaging and multiple arrivals [50] where the computation of multivalued solutions are essential. Recently there has been an increasing interest in designing efficient methods being able to capture multivalued physical variables instead of the viscosity solution: see [47, 17, 18, 26, 49, 20, 43]. The techniques discussed in this paper are based on the physical space, thus offer greater efficiency compared with the computation in the phase space. However, when the number of phases becomes very large, the moment systems become very complex and a hybrid method that combines the low phase number moment system and the Liouville equation would certainly be desirable.

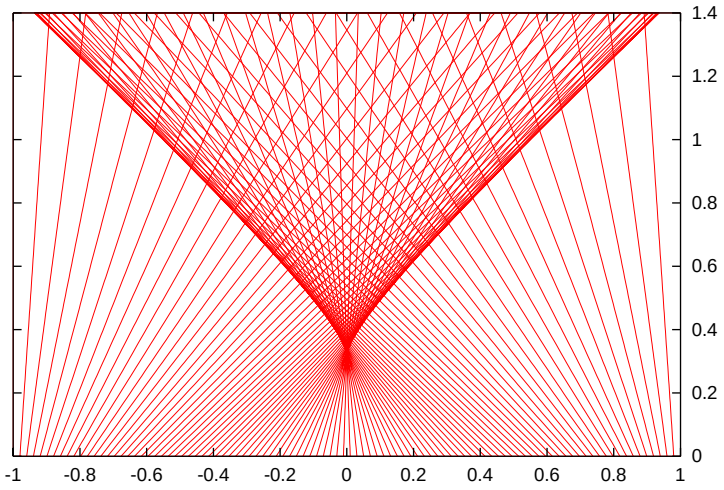

FIGURE 2. Characteristics for (53) with $p = 1$.

ACKNOWLEDGMENT

Part of this work has been achieved during the time the first author was visiting the Mathematics Department at University of Wisconsin-Madison.

REFERENCES

[1] D. Amadori, L. Gosse & G. Guerra, *Global BV entropy solutions and uniqueness for hyperbolic systems of balance laws*, Arch. Rational Mech. Anal. **162** (2002) 327–366.

[2] F. Bouchut, On zero pressure gas dynamics, Advances in Kinetic Theory and Computing, Selected Papers, Series on Advances in Mathematics for Applied Sciences 22 (1994), 171-190, World Scientific.

[3] W.Z. Bao, Shi Jin and P.A. Markowich, On time-splitting spectral approximations for the Schrödinger equation in the semiclassical regime, J. Comp. Phys. **175** (2002), 487-524.

[4] J-D. Benamou, Big ray tracing: Multivalued travel time field computation using viscosity solution of the eikonal equation, J. Comp. Phys.,128(4), 463-474, 1996.

[5] J-D. Benamou,Direct computation of multivalued phase space solutions for Hamilton-Jacobi equations, Comm. Pure Appl. Math.,52(11), 1443-1475,1999.

[6] A.P. Blanc, G.T. Kossioris, G.N. Makrakis, *Geometrical optics and viscosity solutions*, in "Numerical methods for viscosity solutions and applications" (2001) World Sci. Publishing, 1– 20.

[7] F. Bouchut and F. James, *One-dimensional transport equations with discontinuous coefficients*, Nonlinear Analysis TMA, **32** (1998), 891 – 933.

[8] F. Bouchut and F. James, *Duality solutions for pressureless gases, monotone conservation laws and uniqueness*, Comm. P.D.E. **24** (1999) 2173–2189.

[9] F. Bouchut, Shi Jin and X.T. Li, Numerical approximations of pressureless gas and isothermal gas dynamics, to appear in SIAM J. Numer. Anal.

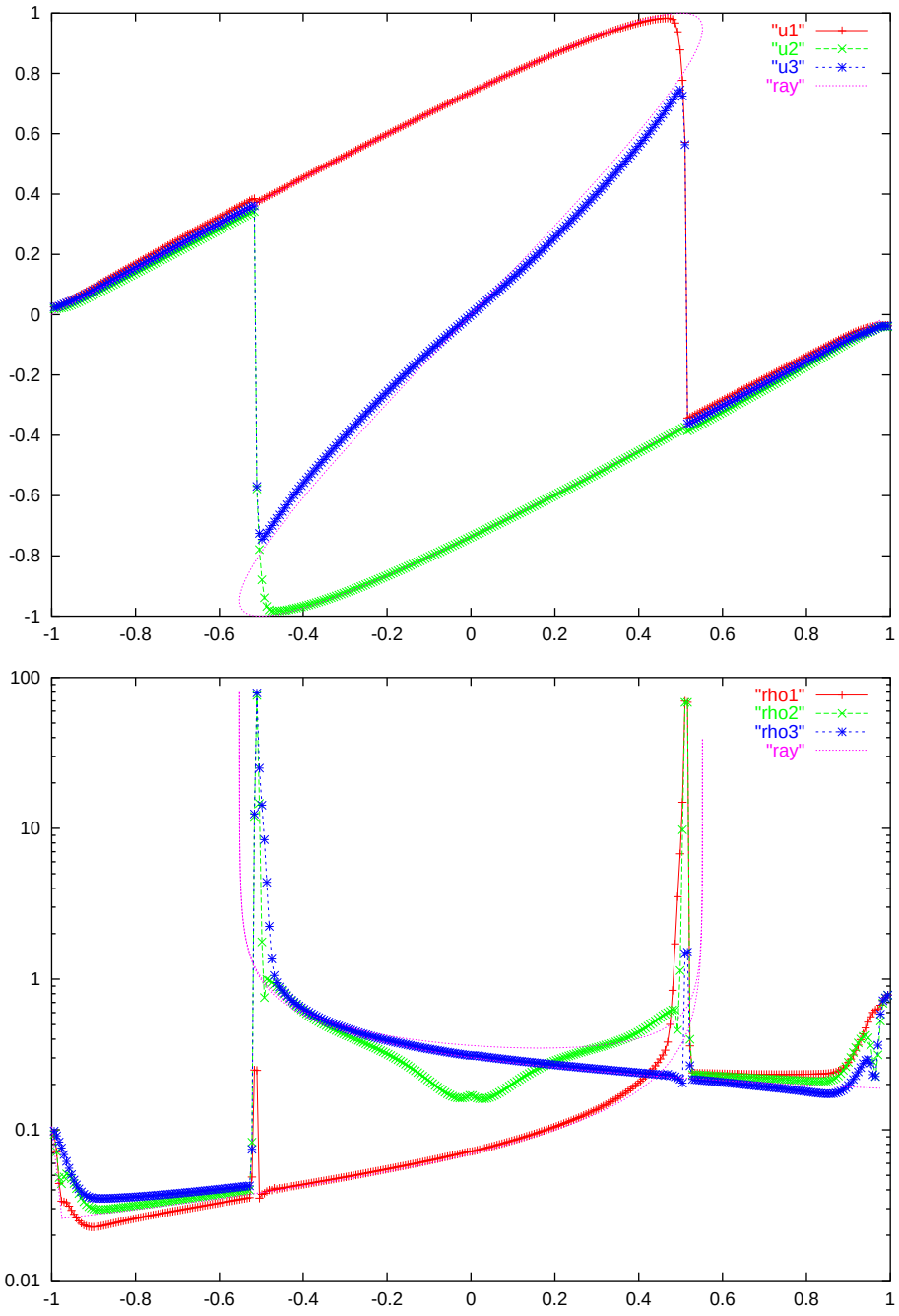

FIGURE 3. Numerical results for $u_{1,2,3}$ (top) and $\rho_{1,2,3}$ (bottom) at time $T = 1$ with (32), $K = 3$ and $p = 1$.

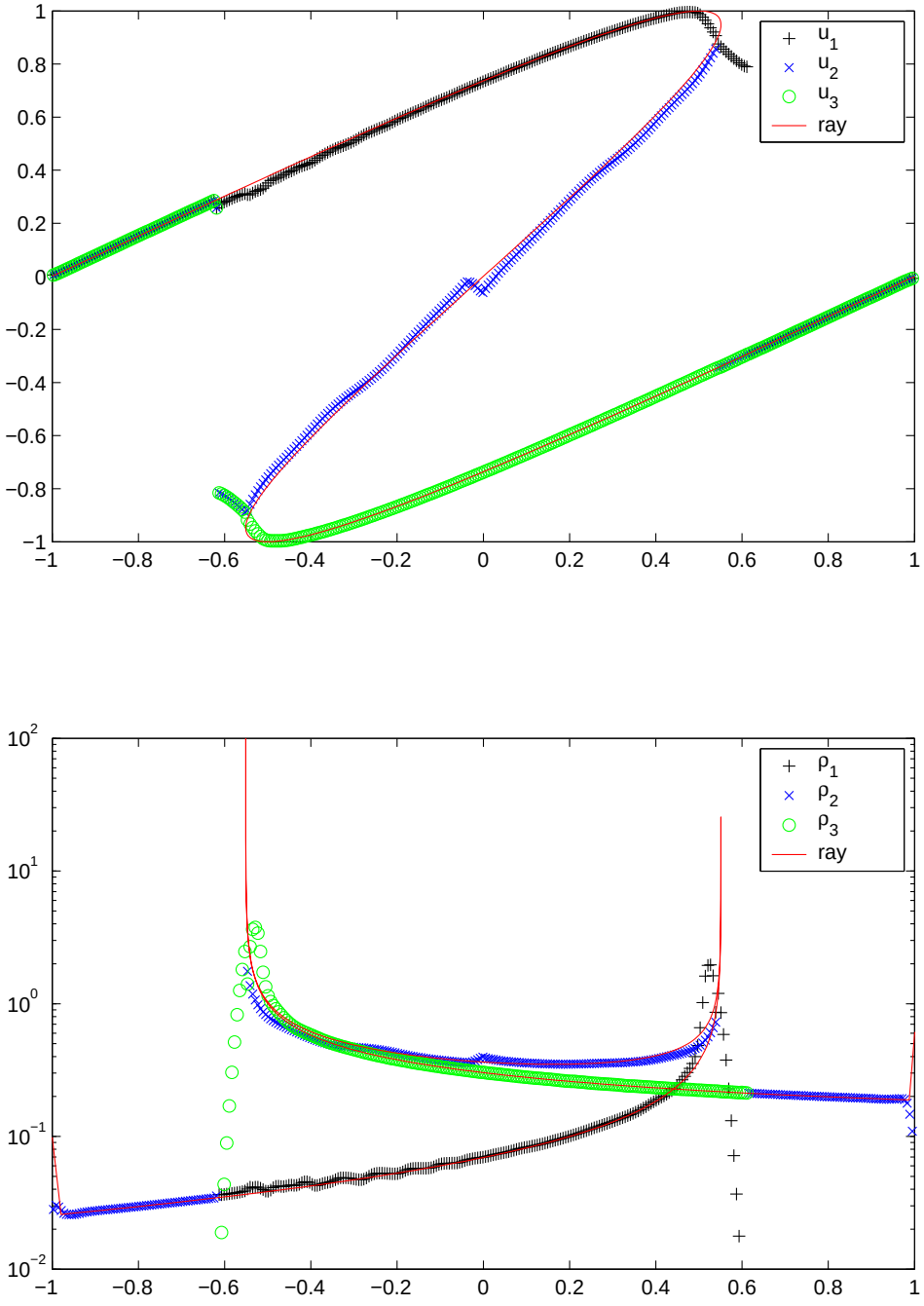

FIGURE 4. Numerical results for $u_{1,2,3}$ (top) and $\rho_{1,2,3}$ (bottom) at time $T = 1$ with (20), $N = 3$ (second order) and $p = 1$.

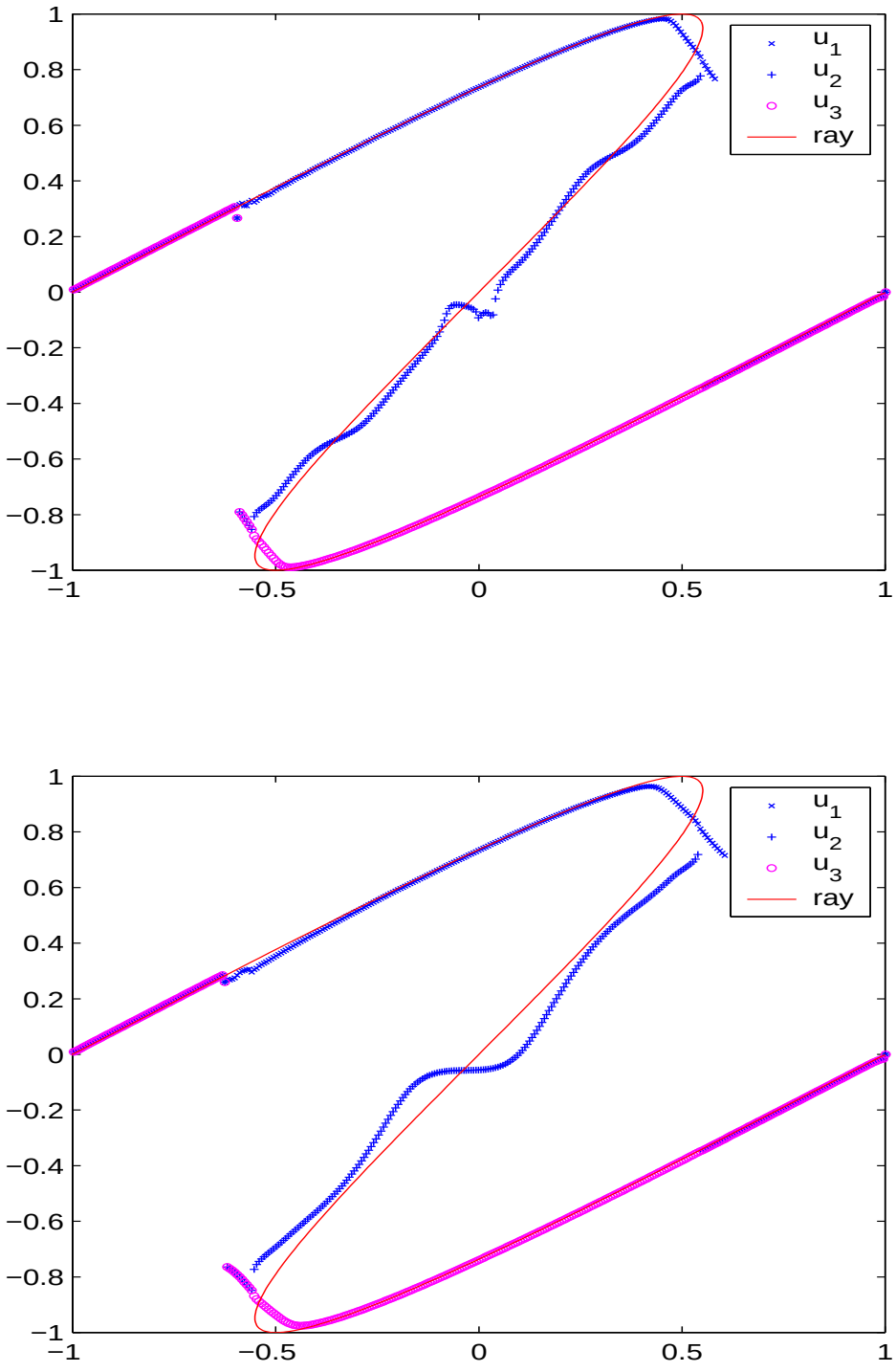

FIGURE 5. Comparison between the first order kinetic scheme (above) and the first order Local Lax Friedrichs scheme(below) for the three-phase δ system (20). $p = 1$.

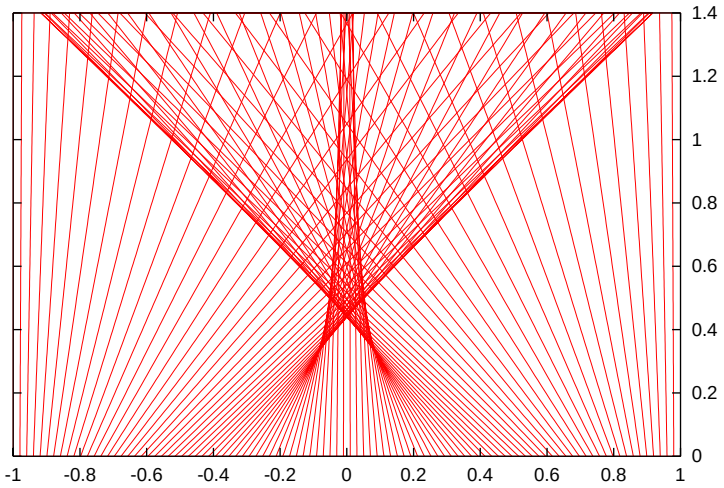

FIGURE 6. Characteristics for (53) with $p = 2$.

[10] Y. Brenier, *Averaged multivalued solutions for scalar conservation laws*, SIAM J. Numer. Anal. **21** (1984), 1013 – 1037.
[11] Y. Brenier and L. Corrias, Capturing multi-valued solutions, UCLA CAM Report 94-46.
[12] Y. Brenier and L. Corrias, A kinetic formulation for multibranch entropy solutions of scalar conservation laws, Ann. Inst. Henri Poincaré, 15(2): 169-190, 1998.
[13] Y. Brenier, E. Grenier, Sticky particles and scalar conservation laws, SIAM J. Num. Anal. 35 (1998), 2317-2328.
[14] P. CARGO AND A.Y. LEROUX, *Un schéma équilibre adapté au modèle d'atmosphère avec termes de gravité*, C.R. Acad. Sc. Paris Série I, 318 (1994), pp. 73 – 76.
[15] M. Crandall, P.L. Lions, *Viscosity solutions of Hamilton-Jacobi equations*, Trans. Amer. Math. Soc. **282** (1984), 487 – 502.
[16] M. Crandall, P.L. Lions, *Two approximations of viscosity solutions of Hamilton-Jacobi equations*, Math. Comp. **43** (1984), 1 – 19.
[17] B. Engquist and O. Runborg, Multi-Phase computations in geometrical optics, J. Comp. Appl. Math. 74 (1996), 175-192.
[18] B. Engquist, O. Runborg and A.-K. Tornberg, High frequency wave propagation by the segment projection method, J. Comp. Phys. 178 (2002) 373–390.
[19] E. Fatemi, B. Engquist and S. Osher, Numerical solution of the high frequency asymptotic expansion for the scalar wave equation, J. Comput. Phys., 120(1): 145-155, 1995.
[20] S. Fomel and J.A. Sethian, Fast-phase space computation of multiple arrivals, PNAS, Vol. 99, no. 11, 7329-7334, 2002.
[21] I. Gasser, C.K. Lin & P.A. Markowich, A review of dispersive limits of (non)linear Schrödinger-type equations, Taiwanese J. Math. (2000) 501-529.
[22] P. Gerard, P.A. Markowich, N.J. Mauser, and F. Poupaud. Homogenization limits and Wigner transforms, Comm. Pure Appl. Math., 50(4), 323-379,1997.
[23] P. Goatin, *One-sided estimates and uniqueness for hyperbolic systems of balance laws*, M^3AS, to appear (2002).

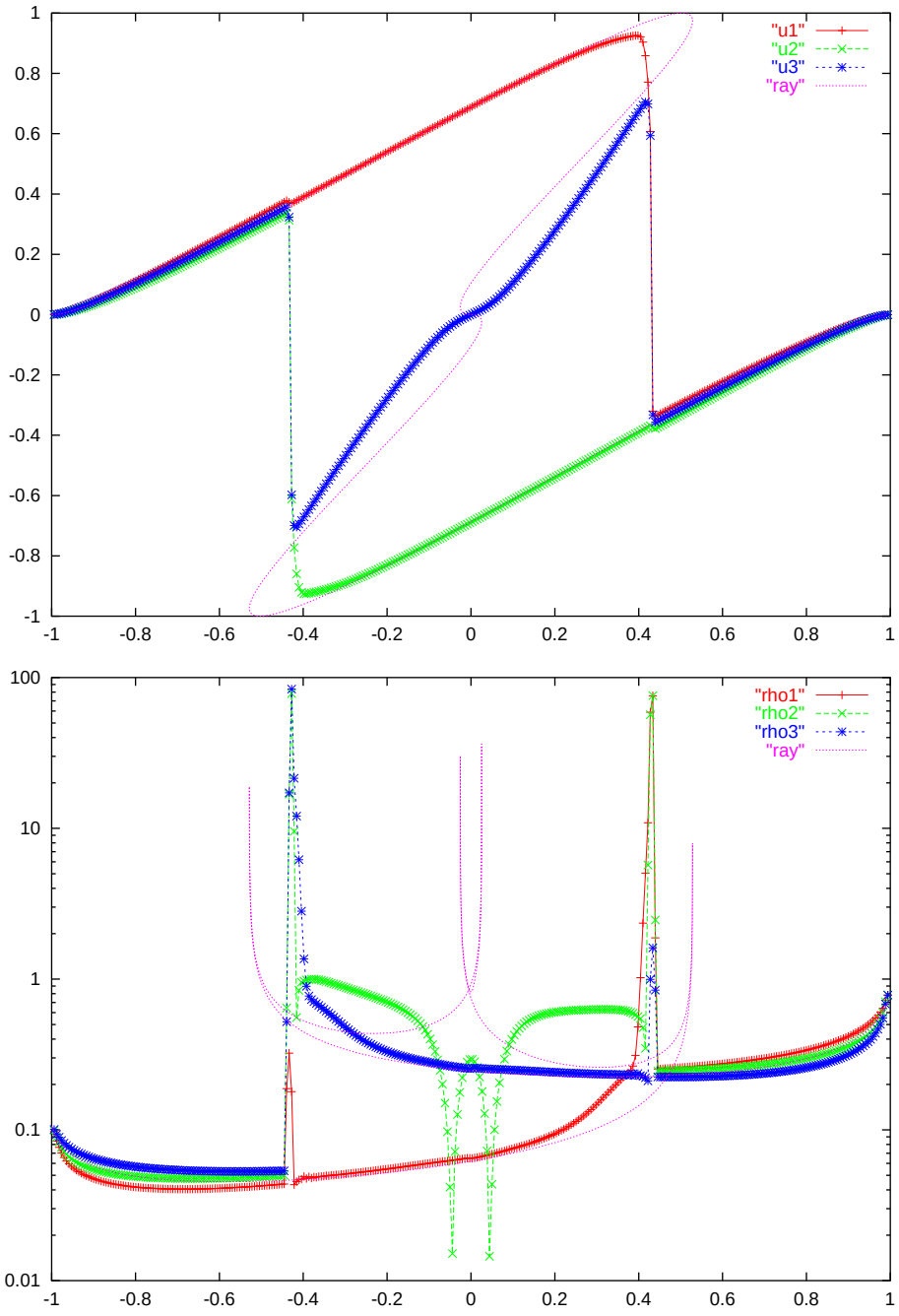

FIGURE 7. Numerical results for $u_{1,2,3}$ (top) and $\rho_{1,2,3}$ (bottom) at time $T = 1$ with (32), $K = 3$ and $p = 2$.

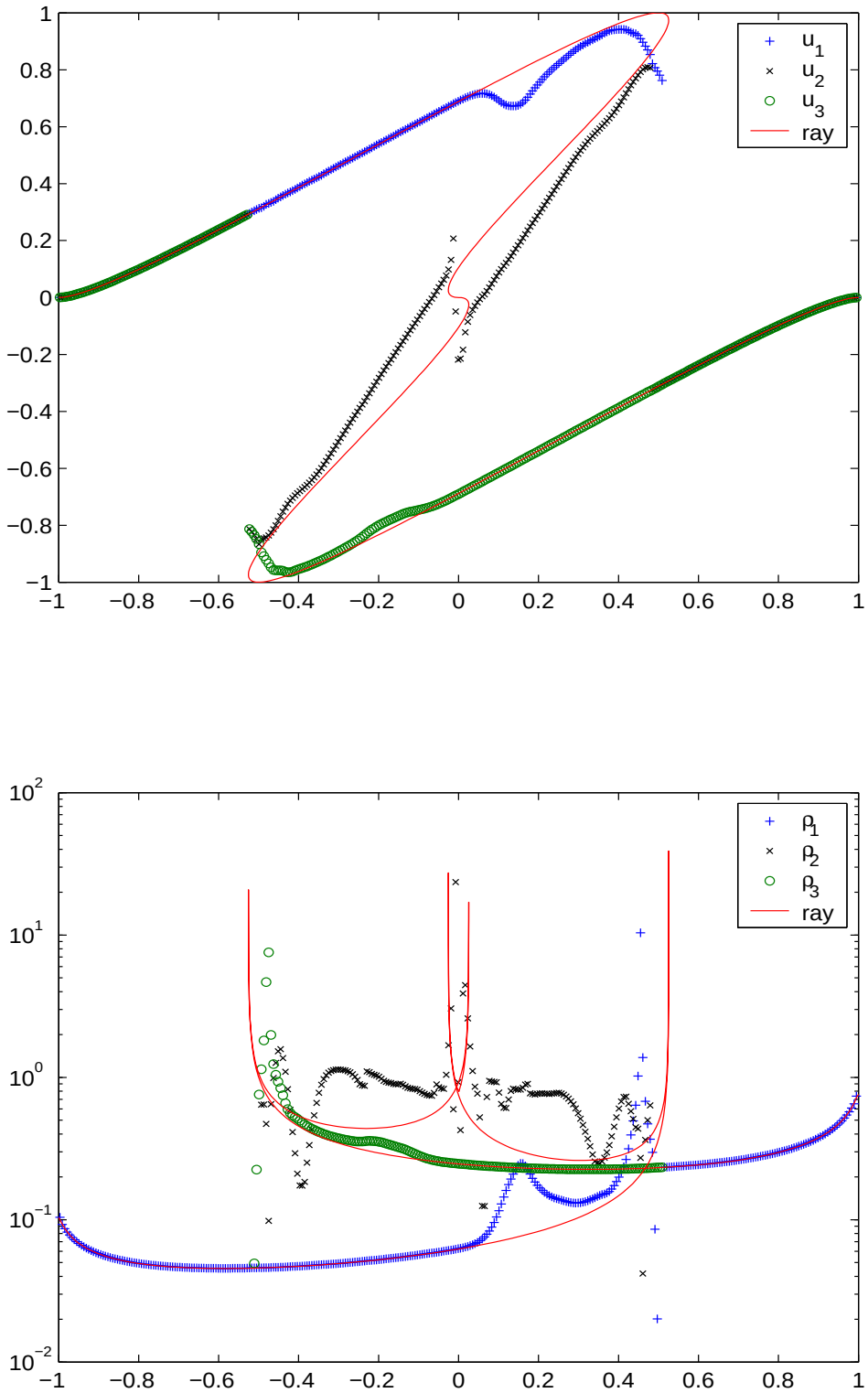

FIGURE 8. Numerical results for $u_{1,2,3}$ (top) and $\rho_{1,2,3}$ (bottom) at time $T = 1$ with (20), $N = 3$ and $p = 2$.

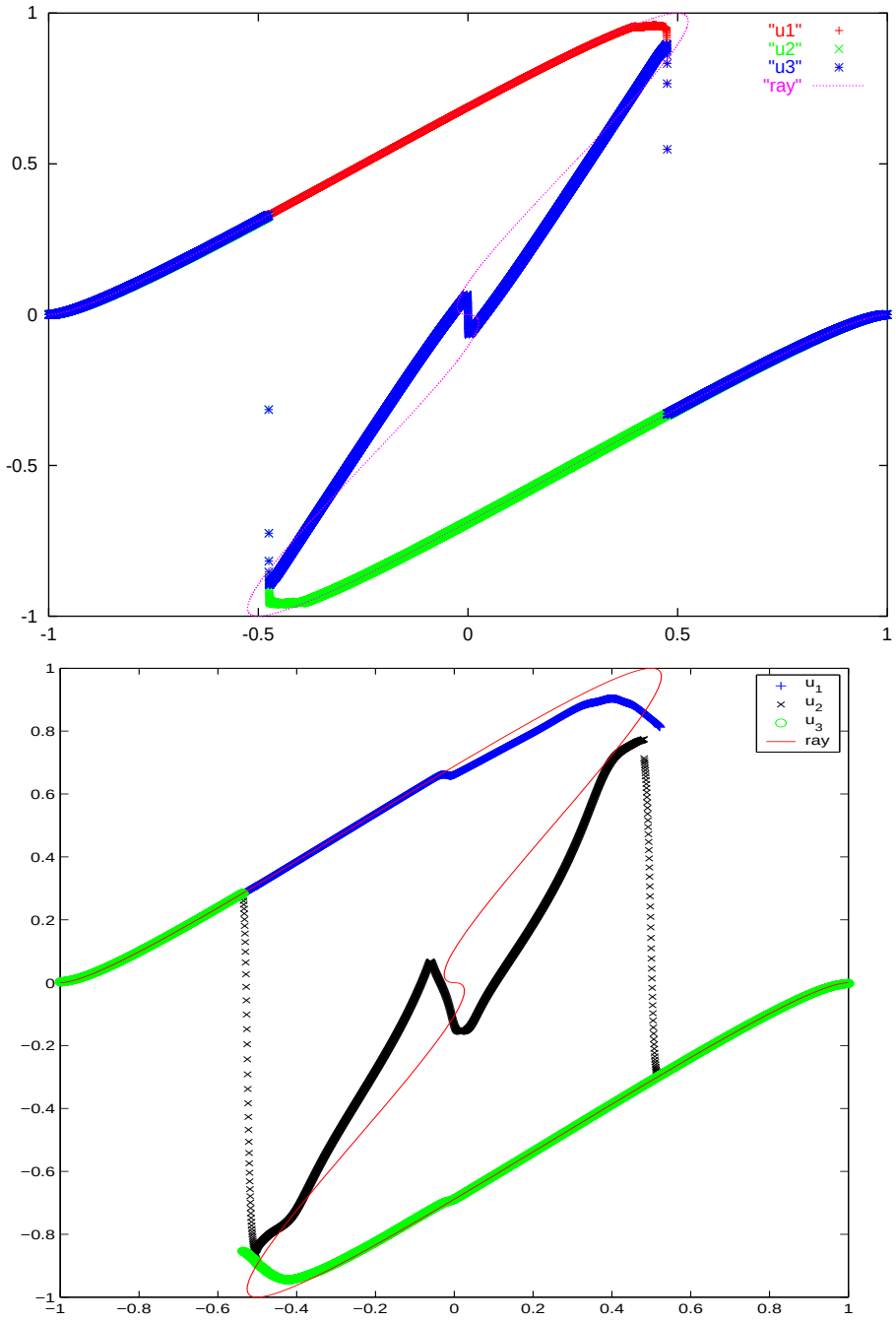

FIGURE 9. Numerical results for $u_{1,2,3}$ with (36) (top) and with (20) (bottom) at time $T = 1$, $K = 3$ and $p = 2$, using a refined calculation ($\Delta x = 0.0006$).

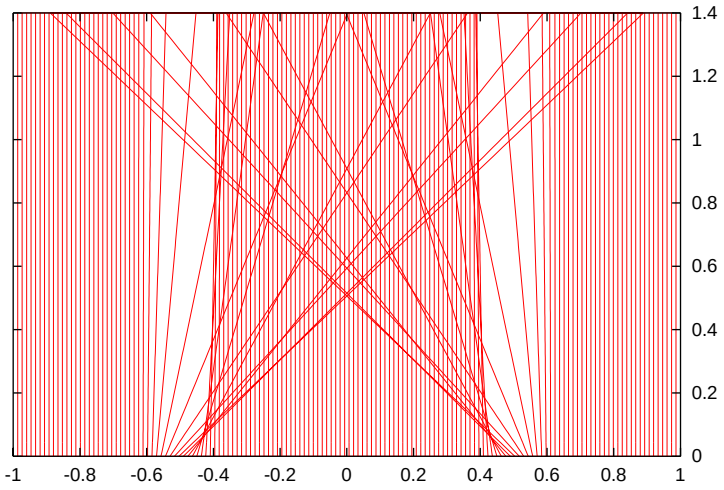

FIGURE 10. Characteristics for (53) with $p = 100$.

[24] L. GOSSE, *A well-balanced flux splitting scheme designed for hyperbolic systems of conservation laws with source terms*, Comp. Math. Applic. **39** (2000) 135 – 159.

[25] L. Gosse, *A nonconservative approach for hyperbolic systems of balance laws: the well-balanced schemes*, in "Hyperbolic problems: theory, numerics, computations", H. Freistuhler & G. Warnecke Eds. Birkhaüser Verlag INSM **140** (2002) 453–461.

[26] L. Gosse, *Using K-branch entropy solutions for multivalued geometric optics computations*, J. Comp. Phys., Vol. **180**, No. 1, (2002), 155–182.

[27] L. Gosse & F. James, *Numerical approximations of one-dimensional linear conservation equations*, Math. Comp. **69** (2000), 987 – 1015.

[28] L. Gosse & F. James, *The viscosity-duality solutions approach to geometric optics for the Helmholtz equation*, in "Numerical methods for viscosity solutions and applications" (2001) World Sci. Publishing, 133 – 152.

[29] L. Gosse & F. James, *Convergence results for an inhomogeneous system arising in various high frequency approximations*, Numer. Math. **90** (2002), 721 – 753

[30] J. GREENBERG AND A.Y. LEROUX, *A well balanced scheme for the numerical processing of source terms in hyperbolic equations*, SIAM J. Numer. Anal., 33 (1996) pp. 1 – 16.

[31] E. Grenier, *Semiclassical limit of the nonlinear Schrödinger equation in small time*, Proc. A.M.S. **126** (1998) 523–530.

[32] Shan Jin, C.D. Levermore and D.W. Mclaughlin, The semiclassical limit of the defocusing NLS Hierarchy, Comm. Pure Appl. Math., 52(1999), 613-654.

[33] Shi Jin, *A steady-state capturing method for hyperbolic systems with geometrical source terms*, Math. Model Num. Anal. **35** (2001), 631-645.

[34] Shi Jin, X.T. Li, *Multi-phase computations of the semiclassical limit of the Schrödinger equation and related problems: Whitham vs. Wigner*, submitted to Physica D.

[35] J. Keller, *Semiclassical mechanics*, SIAM review **27** (1985), 485 – 504.

[36] P.G. LEFLOCH AND A.E. TZAVARAS, *Representation of weak limits and definition of nonconservative products*, SIAM J. Math. Anal. 30 (1999), pp. 1309–1342.

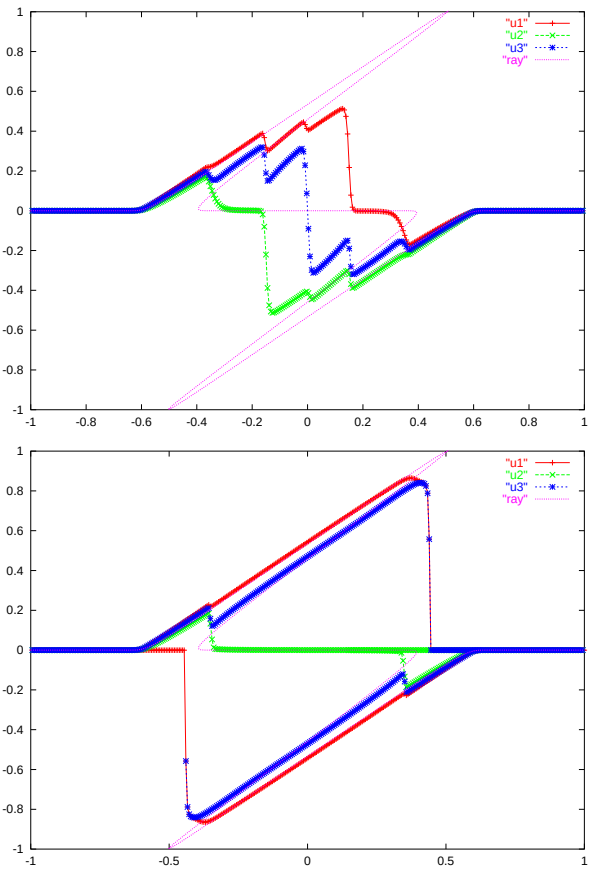

FIGURE 11. Numerical results for $u_{1,2,3}$ with (32), $K = 3$ and $p = 100$ at time $T = 0.5$ using symmetry (bottom) or not (top).

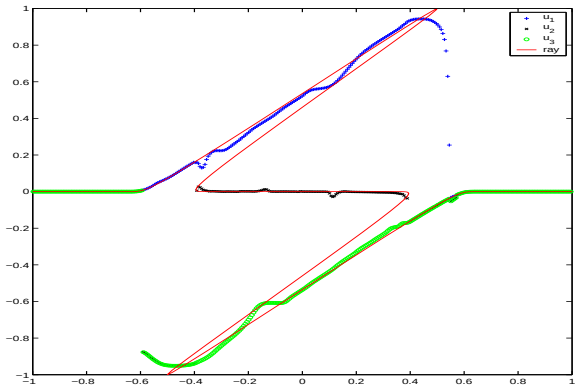

FIGURE 12. Numerical results for $u_{1,2,3}$ at time $T = 1$ with (20), $N = 3$ and $p = 100$.

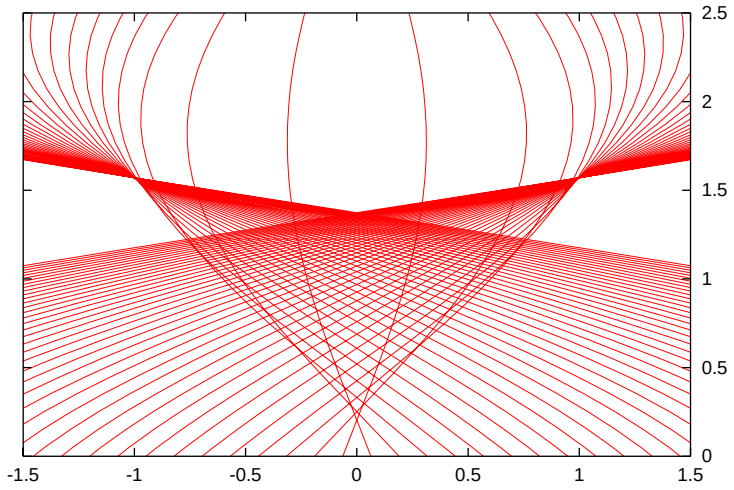

FIGURE 13. Characteristics for (54) and $V(x) = \frac{1}{2}x^2$.

[37] X.T. Li, PhD thesis, University of Wisconsin-Madison, 2002.
[38] P.L. Lions and T. Paul, Sur les measures de Wigner, Revista. Mat. Iberoamericana 9, 1993, 553-618.
[39] P.L. Lions, B. Perthame, E. Tadmor, *A kinetic formulation of multidimensional scalar conservation laws and related equations*, J. Amer. Math. Soc. **7** (1994), 169 – 191.
[40] P.L. Lions, B. Perthame, E. Tadmor, *Kinetic formulation of the isentropic gas dynamics and p-systems*, Comm. Math. Phys. **163** (1994), 415 – 431.
[41] E. Madelung, Quantetheorie in Hydrodynamischer Form, Z. Physik 40 (1927) p.322.
[42] P.A. Markowich, P. Pietra and C. Pohl, Numerical approximation of quadratic observables of Schrödinger-type equations in the semiclassical limit, Numer. Math. 81, 595-630, 1999.
[43] S. Osher, L.T. Cheng, M. Kang, H. Shim and Y.H. Tsai, Geometric optics in a phase space based level set and Eulerian framework, preprint, 2001.
[44] G. Papanicolaou and L. Ryzhik, *Waves and transport*, (Park City,UT, 1995), 305–382, IAS/Park City Math. Ser., **5**, Amer. Math. Soc., Providence, RI, (1999).
[45] B. Perthame, C. Simeoni, *A kinetic scheme for the Saint-Venant system with a source*, CALCOLO **38** (2001), 201 – 231.
[46] J. Rauch and M. Keel, *Lectures on geometric optics. Hyperbolic equations and frequency interactions*, (Park City,UT, 1995), 383-466, IAS/Park City Math. Ser., **5**, Amer. Math. Soc., Providence, RI, (1999).
[47] O. Runborg, Some new results in multi-phase geometrical optics, Math. Model Num. Anal. **34** (2000), 1203-1231.
[48] C. Sparber, P. Markowich, N. Mauser, Multivalued Geometrical optics: Wigner vs. WKB, to appear in Asymptotic Analysis.
[49] W.W. Symes and J. Qian, *A slowness matching Eulerian method for multivalued solutions of Eikonal equations*, submitted to J. Sci. Comp.
[50] J. van Trier and W. W. Symes. Upwind finite-difference calculation of traveltimes, Geophysics, 56(6):812-821, June 1991.

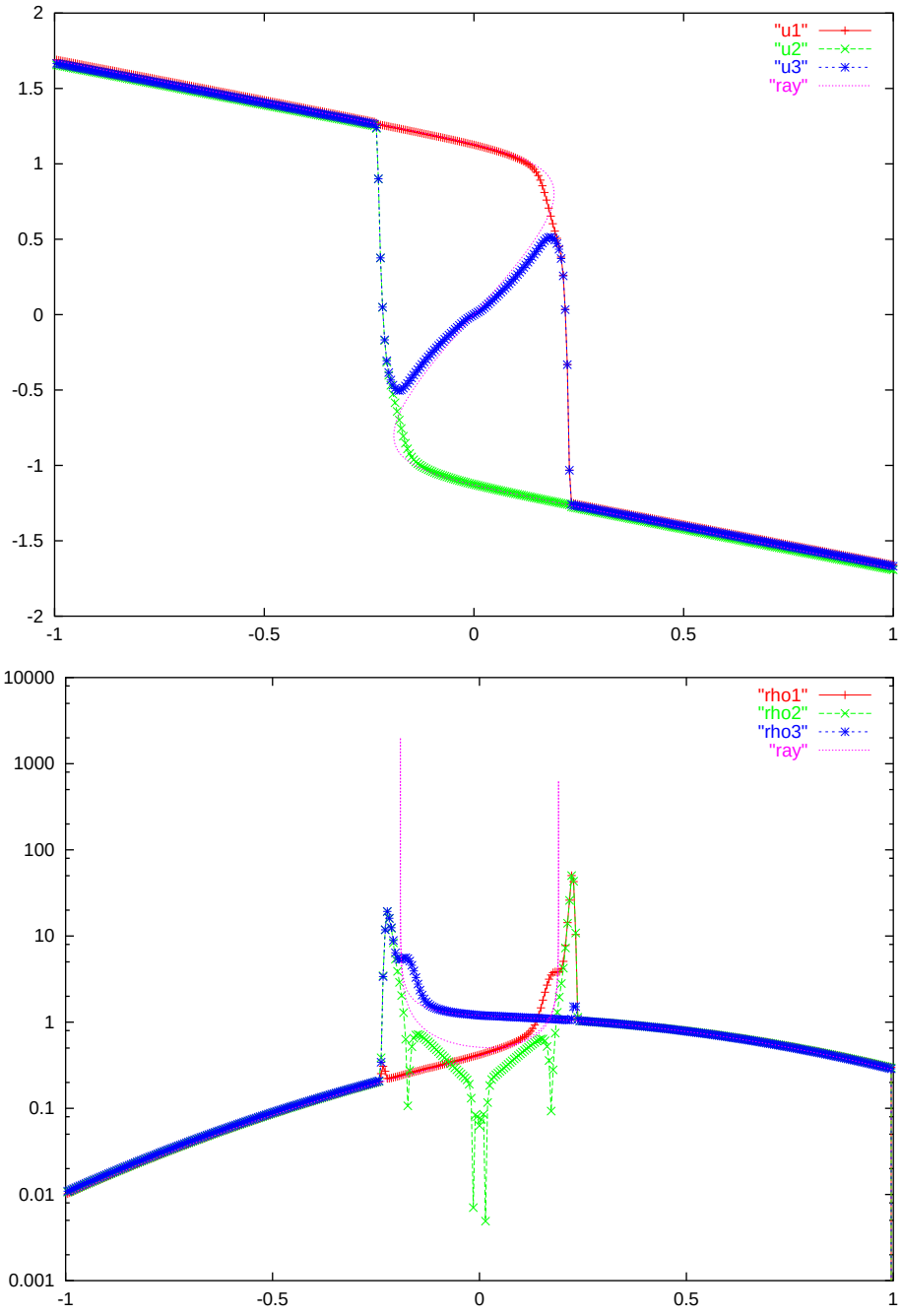

FIGURE 14. Numerical results for $u_{1,2,3}$ (top) and $\rho_{1,2,3}$ (bottom) at time $T = 0.5$ with (32), $K = 3$ and $V(x) = \frac{1}{2}x^2$.

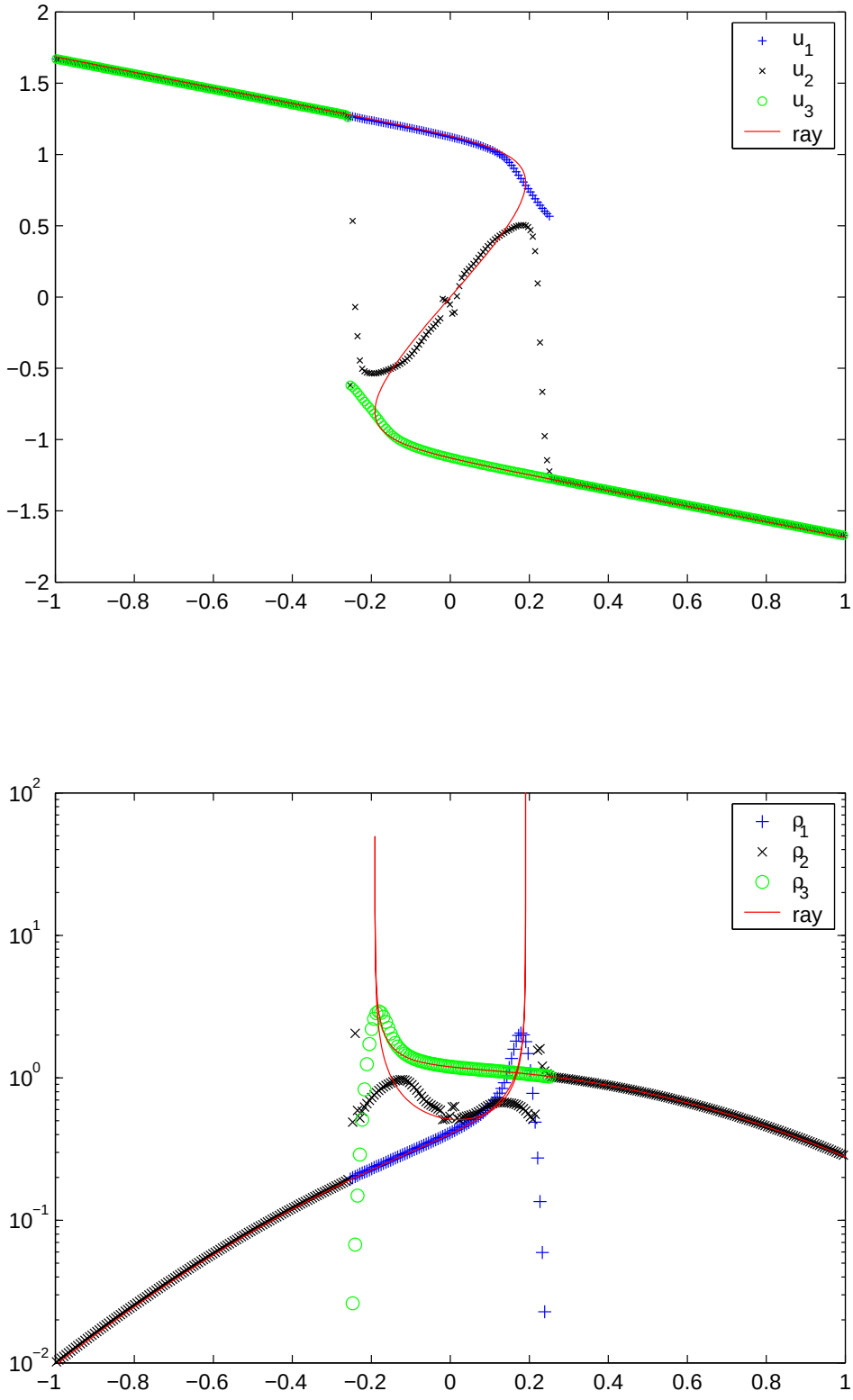

FIGURE 15. Numerical results for $u_{1,2,3}$(top) and $\rho_{1,2,3}$ at time $T = 0.5$ with (20), $N = 3$ and $V(x) = \frac{1}{2}x^2$.

[51] A. Vasseur, *Time regularity for the system of isentropic gas dynamics with* $\gamma = 3$, Comm. P.D.E. **24** (1999), 1987 – 1997.
[52] G.B. Whitham, Non-linear dispersive waves, Proc. Roy. Soc Ser. A283(1965),238-261.
[53] E. Wigner, On the quantum correction for thermodynamic equilibrium, Physical Rev., 40, 1932, 749-759.

Istituto per le Applicazioni del Calcolo (sezione di Bari), Via Amendola 122/I, 70126 Bari (ITALY)
E-mail address: l.gosse@area.ba.cnr.it

Department of Mathematics, University of Wisconsin-Madison, WI 53706 (USA).
E-mail address: jin@math.wisc.edu, xli@math.wisc.edu.